





Regression analysis of the nuclear symmetry energy for relativistic mean-field models

Ilona Bednarek ^{1,*} Wiesław Olchawa ^{2,†} Jan Śladkowski ^{1,‡} and Jacek Syska ^{1,§}

¹*Institute of Physics, University of Silesia, 75 Pułku Piechoty 1, 41-500 Chorzów, Poland*

²*Institute of Physics, University of Opole, Oleska 48, 45-052 Opole, Poland*



(Received 14 June 2022; accepted 14 October 2022; published 17 November 2022)

Regression analysis for the symmetry energy within a sample of relativistic mean-field models of nuclear matter is performed. The selected models consistently meet the experimentally obtained limitations. A proposed measure of the importance of adding the fourth-order term to the symmetry energy is analyzed. As a result of the research, it became possible to arrange the models and perform two-dimensional and one-dimensional linear regression analyses. The one-dimensional regression analysis between the input parameters confirms the appropriateness of introducing the division of the sample of considered models into four separate classes representing four statistically different fits. An additional result is the formulation of constraints on the function, which describes the energy density of the system. The performed two-dimensional regression analysis refers to an alternative method of parametrizing the symmetry energy using the power law. It was found that the Akaike information criterion of model selection involving the γ exponent is sensitive to splitting the symmetry energy into the kinetic and potential parts. The analysis indicates that the more appropriate way of splitting is the one that does not consider the interaction with the sigma meson in the kinetic part.

DOI: [10.1103/PhysRevC.106.055805](https://doi.org/10.1103/PhysRevC.106.055805)

I. INTRODUCTION

Various theoretical strategies and associated numerical techniques have been developed to attack the many-body problem of isospin-asymmetric nuclear matter. Primary methods of tackling fall into three main categories: the many-body microscopic approach, the effective-field theory approach, and the phenomenological approach [1–3]. Theoretical efforts must be confirmed experimentally, utilizing heavy-ion collision experiments and astrophysical measurements. By creating appropriate conditions, experiments with heavy-ion collisions [4–6] make it possible to study extreme states of strongly interacting matter and obtain information about the nuclear equation of state (EoS) at high baryon densities and temperature. This is of great importance to nuclear physics because it allows one to test the understanding of the fundamental aspects of strong interactions. This issue is also important astrophysically concerning the description of the dynamics of supernovae and the properties of neutron stars [7–9]. The EoS of asymmetric nuclear matter is still uncertain, and the main reason for this is a poor understanding of symmetry energy, especially its high-density limit [2,8]. There are many fascinating aspects of the symmetry energy accessible by experimental and theoretical procedures. The basis of the analysis carried out in this paper is the way of defining the symmetry energy, specifically the commonly

used parabolic approximation. Calculations for the analysis in the following sections were based on selected relativistic mean-field (RMF) models. RMF represents an approach to the nuclear matter description understood in a broad aspect of finite nuclei and infinite nuclear matter, emphasizing the matter of a neutron star. The leading type of this category of models is the quantum hadrodynamics (QHD), one whose archetype is the linear Walecka model [10]. In general, QHD develops a framework within which an accurate description of the nuclear many-body problem as a relativistic system of baryons and mesons is provided. QHD is an effective-field theory that describes interacting nucleons based on the mean-field approximation. The original Walecka model describes the properties of nuclear matter by the scalar-isoscalar σ (attractive) and vector-isoscalar ω mesons (repulsive) exchange [11]. This model was then extended by including the vector-isovector ρ meson. This type of model has undergone further modifications, resulting in its increased applicability. Much more sophisticated forms of models include a variety of nonlinear meson interactions [12]. A wide range of these models can be categorized according to interaction terms' parameters. In general, nonlinear interactions between mesons can be divided into representative classes, including self- and mixed-interaction terms [13,14]. Detailed dynamics of individual models are refined by selecting the appropriate Lagrangian function, with parameters that should be compatible with experimental observations. Details are given in Sec. III. Despite many theoretical and experimental efforts, the uncertainty of the density dependence of the symmetry energy, especially its high-density behavior, persists as one of the most challenging problems in nuclear physics [15,16]. The EoS of asymmetric nuclear matter in terms of its binding

*ilona.bednarek@us.edu.pl

†wolch@uni.opole.pl

‡jan.sladkowski@us.edu.pl

§jacek.syska@us.edu.pl

energy per nucleon is a function of baryon number density $n_b = n_n + n_p$, where n_n and n_p are neutron and proton number densities, and the parameter $\delta = (n_n - n_p)/(n_n + n_p)$ which quantifies the isospin asymmetry of the system

$$E(n_b, \delta) = \frac{\varepsilon(n_b, \delta)}{n_b} - M, \quad (1)$$

where $\varepsilon(n_b, \delta)$ denotes the energy density and M is the nucleon mass. One can extract information about the EoS from the Maclaurin expansion of the function $E(n_b, \delta)$ around $\delta = 0$ [17]

$$E(n_b, \delta) = \sum_{k=0}^{\infty} E_{2k}(n_b) \delta^{2k} = E_0(n_b) + \sum_{k=1}^{\infty} E_{2k}(n_b) \delta^{2k}, \quad (2)$$

where $E_0 = E(n_b, \delta = 0)$ is the energy of symmetric nuclear matter, and all components of the sum in Eq. (2) beyond the term E_0 determine the isospin asymmetric part of the binding energy. Thus, the expansion (2) aims to indicate the system's dependence on isospin asymmetry. Depending on the ratio of the number of protons and neutrons, the system can exist in states of different energies. Information about energy differences associated with conditions characterized by other numbers of neutrons and protons, therefore differing in the value of the δ parameter, is provided by the asymmetry energy

$$E_{\text{asym}}(n_b, \delta) = E(n_b, \delta) - E_0(n_b). \quad (3)$$

In general, the nuclear symmetry energy is defined as the difference between the energy of neutron matter and symmetric nuclear matter,

$$E_{\text{sym}}(n_b) = E(n_b, \delta = 1) - E(n_b, \delta = 0), \quad (4)$$

and can be identified with the appropriate coefficient in the Maclaurin series (2). The Maclaurin series truncated to the second-order leads to the commonly used parabolic approximation of the EoS,

$$E(n_b, \delta) = E_0(n_b) + \frac{1}{2} \left. \frac{\partial^2 E}{\partial \delta^2} \right|_{\delta=0} \delta^2 + \dots. \quad (5)$$

In this case, the symmetry energy $E_{\text{sym}}(n_b)$ is equated with satisfactory accuracy as the coefficient E_2 of the series (2). When the quartic term is included, the sum of E_2 and E_4 is accepted as being the valid approximation. The quantity $E_2(n_b) \delta^2$ for the parabolic approximation determines the asymmetry-energy contribution to the energy $E(n_b, \delta)$.

The density dependence of the nuclear matter EoS is expressed in terms of coefficients that appear in the Taylor-series expansion of functions $E_0(n_b)$ and $E_{\text{sym}}(n_b)$ around the saturation density n_0 . The results obtained for symmetric nuclear matter in the case of parabolic approximation can be written as

$$E_0(n_b) = E_0(n_0) + \frac{K_0}{2} \left(\frac{n_b - n_0}{3n_0} \right)^2 + \dots, \quad (6)$$

where E_0 is the binding energy, and K_0 is the incompressibility of symmetric nuclear matter, both taken at n_0 . The density dependence of the symmetry energy is specified by the

expression

$$E_{\text{sym}}(n_b) = E_{\text{sym}}(n_0) + L_0 \left(\frac{n_b - n_0}{3n_0} \right) + \frac{K_{\text{sym}}}{2} \left(\frac{n_b - n_0}{3n_0} \right)^2 + \dots, \quad (7)$$

where E_{sym} , L_0 , and K_{sym} denote the symmetry-energy coefficient, its slope, and its curvature, respectively. All coefficients are also calculated at the saturation density n_0 . Sustained experimental and theoretical efforts are made to put constraints on particular coefficients and provide the optimal parametrizations of models describing nuclear matter. Determination of reliable constraints on the parameters characterizing the isospin-dependent part of the nuclear matter equation of state is a formidable experimental challenge. Depending on the density range achieved in the given experiment, different observables can be used for this purpose. The most satisfactory results were obtained for the saturation density based on the data analysis obtained with the use of observables that include, among others, the atomic masses [18], neutron skins of heavy nuclei [19], isospin diffusion in heavy-ion reactions [20], excitation energies of isobaric-analog states (IAS) [21], isoscaling of fragments from intermediate energy heavy-ion collisions [22], the electric-dipole polarizability from analyzing the Pygmy dipole resonance [23], the frequency of isovector giant dipole resonances [24], and optical potentials from studying nucleon-nucleus scatterings [25,26]. The development of experimental techniques and theoretical methods offers varying approaches to understanding the dependence of the symmetry energy on density. Of considerable importance are the results obtained in the lead radius experiment (PREX). The reported updated results give the value of the neutron skin thickness $\Delta r_{\text{np}}^{208} = 0.283 \pm 0.071$ fm [27–29]. This experimental finding is particularly vital not only for the nuclear structure but also as a tool to probe the properties of the symmetry energy. Different theoretical approaches indicate that the size of neutron skin in ^{208}Pb and the value of the symmetry-energy slope $L(n_b)$ are linearly related with the most substantial value of the correlation at the subsaturation cross density $n_c = 2/3 n_0$ [30], which approximately corresponds to the average density of atomic nuclei. The symmetry energy slope $L(n_b)$ in the vicinity of the saturation density n_0 influences the mass-radius relation and tidal deformability of neutron stars [27,31–34], thus the thickness of the neutron skin of heavy nuclei and the radii of neutron stars are among the most promising observables that convey information about symmetry energy. At the same time, they also allow the determination of neutron-star parameters. Observables describing nuclei's collective motions in nuclear reactions are used to probe the symmetry-energy properties for densities higher than the saturation density n_0 , among others [26]. However, the resulting limitations are endowed with much more considerable uncertainties. Experimental verification of the properties of symmetry energy distinguishes observables such as isospin diffusion or neutron-to-proton ratios, the description of which is based on the transport theory [35–37]. A good description of available experimental data is obtained by adopting the power-law to recount the

dependence of energy symmetry on density, which is an alternative form of symmetry energy parametrization. Usually, one separates the symmetry energy into kinetic and potential contributions $E_{\text{sym}}(n_b) = E_{\text{sym}}^{\text{kin}}(n_b) + E_{\text{sym}}^{\text{pot}}(n_b)$. The need to know the potential and kinetic parts of the symmetry energy has its justification in specific nuclear physics problems, for example, in simulations of heavy-ion collisions [38] and astrophysics. Given the astrophysical aspect, it was found that the critical densities for forming four different charge states $\Delta(1232)$ depend differently on the kinetic and potential parts of the symmetry energy [39]. The description of the kinetic part is frequently given based on the free Fermi gas model. Using the power-law parametrization for the potential part

$$E_{\text{sym}}^{\text{pot}}(n_b) = E_{\text{sym}}^{\text{pot}}(n_0) \left(\frac{n_b}{n_0} \right)^\gamma \quad (8)$$

results in the following relation for the γ parameter:

$$\gamma = \frac{L_0 - L_0^{\text{kin}}}{3E_{\text{sym}}^{\text{pot}}(n_0)}, \quad (9)$$

where the symmetry energy slope L_0 is defined as

$$L_0 = 3n_0 \left. \frac{dE_{\text{sym}}(n_b)}{dn_b} \right|_{n_0}. \quad (10)$$

The paper is organized as follows: in Sec. II, the inaccuracy of the parabolic approximation of the symmetry energy is determined. The paper uses the approximation method based on the Dyson summation approach. The representation of the symmetry energy as a function generated by the Padé approximants [40] allows the definition of a series of the Dyson type and the use of its properties. The third section presents the theoretical approach to assessing the energy of nuclear matter and describes the parametrization of the sample of the models used. In the fourth section, a two-dimensional regression analysis based on the splitting method of the symmetry energy into the kinetic and potential part is given. The obtained results and their discussion are included in the fifth section. Knowledge about the properties of nuclear matter is obtained indirectly from experiments. Thus their interpretation depends on how reliable are the models involved in explaining the experimental observables. Different classes of models can be used to describe individual observables. If several models overlap in the experimentally acceptable description of the properties of nuclear matter, it becomes possible to narrow down the area of the model parameters.

A set of $N = 23$ RMF models is examined. Their multitude results from the necessity to describe various experimental situations. The study assumes that each of the RMF models separately is reliably estimated by a very large number of real observations. With this assumption, the presented statistical analysis of the set of N RMF models concerns (as if) the study of the experimental reality. Section IV presents a two-dimensional analysis of the regression model selection based on the Akaike information criterion [41], in which attention focuses on the decomposition of the symmetry energy of the model into the kinetic and potential parts. In Sec. V a series of one-dimensional regression analyses for the input parameters ($E_{\text{sym},2}$, L_0 , $E_{\text{sym},4}$, L_4 , n_b , etc.) is performed. On the other

hand, the performed regression analysis allows for the classification of the RMF models, which would be justified even if it concerned only the ordering of the theoretical parameters space of RMF models.

II. THE INACCURACY OF THE PARABOLIC APPROXIMATION TO THE SYMMETRY ENERGY

Critical issues in analyzing the symmetry energy have roots in its implicit-like definition. The customarily applied approach uses the Taylor-series expansion of the nuclear matter EoS because the Taylor series are practical tools for approximating functions that can be difficult to compute otherwise. The series (2) represents the function $E(n_b, \delta_a)$ with satisfactory accuracy in the vicinity of the point $(n_0, 0)$. Moreover, the justification for the parabolic approximation has been verified with good numerical accuracy based on various theoretical models of nuclear matter. Thus, in many cases, the form of the EoS used is based on the parabolic approximation, with E_2 being the dominant term of the asymmetry energy (3). However, doubts about the validity of the parabolic approximation remain in the case of neutron-star matter characterized by extreme values of density and isospin asymmetry. It has been shown that special properties of neutron stars, such as the proton fraction at beta equilibrium, the core-crust transition density, and the critical density for the direct URCA process, are sensitive to the quartic term in the symmetry energy [42,43]. Analysis of the fourth-order symmetry energy term within the selected nonlinear RMF models was performed in Ref. [44]. The authors derived the explicit form of the function $E_{\text{sym},4}(n_b)$ and then studied its corrections to the parabolic law for the isospin asymmetric nuclear matter. Their results confirm that the $E_{\text{sym},4}(n_b)$ influences isospin-dependent properties of nuclear matter, such as the proton fraction in β -stable neutron-star matter and the core-crust transition density and pressure in neutron stars. In general, a finite sum of Taylor terms does not guarantee stable nor systematically improvable approximation to the exact form of the energy density function. The mathematical results suggest that the Padé approximants approach gives a better representation of the original function than the truncated Taylor series [40]. Several algorithms have been developed [45] to compare the effectiveness of the Taylor and Padé methods. Assuming that the function $E_{\text{sym}}^P(n_b, \delta)$ represents the form of the symmetry energy fairly accurately [46,47], and E_2 is its dominant contribution then the fourth-order term E_4 is considered as an amendment. In this case,

$$E(n_b, \delta) = E_0(n_b) + E_{\text{sym}}^P(n_b, \delta)\delta^2, \quad (11)$$

where $E_{\text{sym}}^P(n_b, \delta)\delta^2$ stands for the contribution of [46] the asymmetry energy to the nuclear matter EoS. Introducing the factor $r(n_b)$

$$r(n_b) = E_{\text{sym},4}(n_b)[E_{\text{sym},2}(n_b)]^{-2}, \quad (12)$$

the function $E_{\text{sym}}^P(n_b, \delta)$ can be written in the following way [46]:

$$E_{\text{sym}}^P(n_b, \delta) = \frac{E_{\text{sym},2}(n_b)}{1 - r(n_b)E_{\text{sym},2}(n_b)\delta^2}. \quad (13)$$

Functions $E_{\text{sym},2}(n_b)$ and $E_{\text{sym},4}(n_b)$, for which the exact density dependencies are unknown, set the form of $r(n_b)$. If the parabolic approximation were exact then $r(n_b)$ would vanish, $r(n_b) = 0$, and $E_{\text{sym}}^P(n_b) = E_{\text{sym},2}(n_b)$. The function $w(n_b) = E_{\text{sym},4}(n_b)/E_{\text{sym},2}(n_b)$ measures the importance of the fourth-order symmetry energy contribution and can roughly be understood, in the case of RMF models, as the relative error of the parabolic approximation. In this context, $r(n_b) = E_{\text{sym},4}(n_b)[E_{\text{sym},2}(n_b)]^{-2} = w[E_{\text{sym},2}(n_b)]^{-1}$ can be interpreted as the specific inaccuracy of the parabolic approximation. The product $r(n_b)E_{\text{sym},2}(n_b) = w(n_b)$ carries information about the relative value of the amendment and thus the need to use higher-order terms. Knowing the function $r(n_b)$ through the relationship $E_r(n_b) = 1/r(n_b)$ enables the determination of the corresponding energy scale value $E_r(n_b)$.

The necessity to introduce the fourth-order terms to the description of asymmetric nuclear matter is analyzed by effective methods of the Dyson series type. The symbolic ‘‘Dyson’’ series for $E_{\text{sym}}^P(n_b, \delta)$ is

$$\begin{aligned} E_{\text{sym}}^P(n_b, \delta) &= \frac{E_{\text{sym},2}(n_b)}{1 - r(n_b)E_{\text{sym},2}(n_b)\delta^2} \\ &= E_{\text{sym},2}(n_b) + E_{\text{sym},2}(n_b)[r(n_b)\delta^2]E_{\text{sym},2}(n_b) \\ &\quad + E_{\text{sym},2}(n_b)[r(n_b)\delta^2]^2E_{\text{sym},2}(n_b)[r(n_b)\delta^2] \\ &\quad \times E_{\text{sym},2}(n_b) + \dots \end{aligned} \quad (14)$$

The following analysis was performed on a sample of $N = 23$ RMF models.

The approximate solution to the function $r(n_b)$

The saturation density for each model is denoted by n_0 , which has different values for each RMF model. This model-dependent n_0 will be denoted \tilde{n}_0 . Introducing \tilde{n}_0 , which for a specific model takes the value equal to its saturation density n_0 , the following relation at the first-order approximation in $\Delta n_b \equiv (n_b - \tilde{n}_0)$ can be obtained from Eq. (12)

$$\begin{aligned} r(n_b) &\approx r(\tilde{n}_0) \left(1 - 2\Delta n_b \frac{d \ln E_{\text{sym},2}(\tilde{n}_0)}{dn_b} \right. \\ &\quad \left. + \Delta n_b \frac{d \ln E_{\text{sym},4}(\tilde{n}_0)}{dn_b} \right), \end{aligned} \quad (15)$$

where, in line with Eq. (12), $r(\tilde{n}_0) = E_{\text{sym},4}(\tilde{n}_0)E_{\text{sym},2}^{-2}(\tilde{n}_0)$. Equation (15) can be rewritten in the form:

$$\frac{1}{r(\tilde{n}_0)} \frac{r(n_b) - r(\tilde{n}_0)}{\Delta n_b} \approx \frac{d \ln E_{\text{sym},4}(\tilde{n}_0)}{dn_b} - 2 \frac{d \ln E_{\text{sym},2}(\tilde{n}_0)}{dn_b}. \quad (16)$$

Thus, assuming that the linear approximation in the expansion (15) is satisfactory, the following relation can be obtained

$$\begin{aligned} \frac{1}{r(\tilde{n}_0)} \frac{r(n_b) - r(\tilde{n}_0)}{n_b - \tilde{n}_0} &= \frac{\Delta r(\tilde{n}_0)}{r(\tilde{n}_0)} \frac{1}{\Delta n_b} = - \frac{1}{E_{\text{sym},2}} \frac{dE_{\text{sym},2}(\tilde{n}_0)}{dn_b} \\ &\quad - \frac{E_{\text{sym},4}}{E_{\text{sym},2}} \frac{d}{dn_b} \frac{E_{\text{sym},2}}{E_{\text{sym},4}}(\tilde{n}_0), \end{aligned} \quad (17)$$

where \tilde{n}_0 is a variable that takes values equal to saturation densities for all the considered models. Given a specific model with a saturation density n_0 , Eq. (17) can be rewritten in the following form:

$$\begin{aligned} \frac{\Delta r(n_0)}{r(n_0)} \frac{1}{\Delta n_b} &\approx - \frac{1}{3n_0} \left(\frac{L_0}{E_{\text{sym},2}(n_0)} \right. \\ &\quad \left. + 3n_0 \frac{E_{\text{sym},4}(n_0)}{E_{\text{sym},2}(n_0)} \frac{d}{dn_b} \frac{E_{\text{sym},2}}{E_{\text{sym},4}}(n_0) \right), \end{aligned} \quad (18)$$

where L_0 is the symmetry energy slope (10). Solution to the relation (18) leads to the exponential behavior of $r(n_b)$ for a given model:

$$r^*(n_b) = r_0 e^{[-\frac{1}{3}(\frac{L_0}{E_{\text{sym},2}(n_0)} + C_4(n_0))(\frac{n_b - n_0}{n_0})]}, \quad (19)$$

where $r_0 \equiv r(n_0)$ and

$$C_4(n_0) = 3n_0 \frac{E_{\text{sym},4}}{E_{\text{sym},2}} \frac{d}{dn_b} \frac{E_{\text{sym},2}}{E_{\text{sym},4}}(n_0). \quad (20)$$

The evolutionary form of the obtained solution suggests that a continuation to a broader domain of density might not spoil the accuracy of the approximation. The exponent in (19) is a sum of two components. The first is the ratio of two main parametrization factors describing the density dependence of the symmetry energy $L_0/E_{\text{sym},2}(n_0)$. The second (20) is the correction resulting from both the fourth-order and second-order terms in the Maclaurin expansion (2).

III. THE RELATIVISTIC MEAN-FIELD APPROACH

The following Lagrangian density function specifies the detailed dynamics of the system:

$$\mathcal{L} = \mathcal{L}_0 + \mathcal{L}_{\text{int}}. \quad (21)$$

The Lagrangian density of free baryon and meson fields \mathcal{L}_0 is given by

$$\begin{aligned} \mathcal{L}_0 &= \bar{\psi}(i\gamma^\mu \partial_\mu - M)\psi + \frac{1}{2}(\partial^\mu \sigma \partial_\mu \sigma - m_\sigma^2 \sigma^2) \\ &\quad - \frac{1}{4}F^{\mu\nu}F_{\mu\nu} + \frac{1}{2}m_\omega^2 \omega_\mu \omega^\mu \\ &\quad - \frac{1}{4}\mathbf{B}^{\mu\nu}\mathbf{B}_{\mu\nu} + \frac{1}{2}m_\rho^2 \vec{\rho}_\mu \cdot \vec{\rho}^\mu, \end{aligned} \quad (22)$$

where σ , ω_μ , and $\vec{\rho}_\mu$ represent the scalar-isoscalar σ , vector-isoscalar ω , and vector-isovector ρ meson fields, respectively, and ψ is the isodoublet nucleon field. The field tensors $F_{\mu\nu}$ and $\mathbf{B}_{\mu\nu}$ are defined as $F_{\mu\nu} = \partial_\mu \omega_\nu - \partial_\nu \omega_\mu$ and $\mathbf{B}_{\mu\nu} = \partial_\mu \vec{\rho}_\nu - \partial_\nu \vec{\rho}_\mu$. The interaction Lagrangian density \mathcal{L}_{int} includes the couplings of the standard Yukawa type and provides a variety of nonlinear interactions of meson fields grouped in \mathcal{L}_{NL}

$$\begin{aligned} \mathcal{L}_{\text{int}} &= \bar{\psi} \left[g_\sigma \sigma - \left(g_\omega \omega_\mu + \frac{1}{2} g_\rho \vec{\tau} \cdot \vec{\rho}_\mu \right) \gamma^\mu \right] \psi + \mathcal{L}_{NL}, \quad (23) \\ \mathcal{L}_{NL} &= -\frac{A}{3} \sigma^3 - \frac{B}{4} \sigma^4 + \frac{C}{4} (g_\omega^2 \omega_\mu \omega^\mu)^2 \\ &\quad + g_\sigma g_\omega^2 \sigma (\omega_\mu \omega^\mu) \left(\alpha_1 + \frac{1}{2} \alpha'_1 g_\sigma \sigma \right) \\ &\quad + g_\sigma \sigma g_\rho^2 (\vec{\rho}_\mu \vec{\rho}^\mu) \left(\alpha_2 + \frac{1}{2} \alpha'_2 g_\sigma \sigma \right) \\ &\quad + \frac{1}{2} \alpha'_3 (g_\omega g_\rho)^2 (\omega_\mu \omega^\mu) (\vec{\rho}_\mu \vec{\rho}^\mu). \end{aligned} \quad (24)$$

The solution of the equations of motion that follows from the Lagrange function (21) is at the root of calculating the respective energy of the considered model. All analyses were based on the mean-field approximation, in which the meson fields are separated into classical components and quantum fluctuations. After picking the vacuum expectation value, the quantum fluctuation term vanishes and is not included in the ground state, and only classical components remain:

$$\begin{aligned}\sigma &\rightarrow \langle \sigma \rangle \equiv s, & \omega^\mu &\rightarrow \langle \omega \rangle \equiv \langle \omega_0 \rangle \delta^{\mu 0} \equiv \omega_0, \\ \bar{\rho}^\mu &\rightarrow \langle \rho_3 \rangle \equiv \langle \rho_{0,3} \rangle \delta^{\mu 0} \equiv r_{0,3}.\end{aligned}\quad (25)$$

In this approach, the energy density of the system given as the zero component of the energy-momentum tensor takes the following form:

$$\begin{aligned}\varepsilon &= \frac{1}{2}m_\sigma^2 s^2 + \frac{A}{3}s^3 + \frac{B}{4}s^4 - \frac{1}{2}m_\omega^2 \omega_0^2 \\ &\quad - \frac{C}{4}(g_\omega^2 \omega_0^2)^2 + g_\omega \omega_0 n_b \\ &\quad - \frac{1}{2}m_\rho^2 r_{0,3}^2 + g_\rho r_{0,3} n_{3b} \\ &\quad - g_\sigma s (g_\omega \omega_0)^2 \left(\alpha_1 + \frac{1}{2} \alpha'_1 g_\sigma s \right) - g_\sigma s (g_\rho r_{0,3})^2 \\ &\quad \times \left(\alpha_2 + \frac{1}{2} \alpha'_2 g_\sigma s \right) - \frac{1}{2} \alpha'_3 (g_\omega \omega_0)^2 (g_\rho r_{0,3})^2 \\ &\quad + \sum_{j=n,p} \frac{g}{2\pi^2} \int_0^{k_{Fj}} k^2 \sqrt{k^2 + M_{\text{eff},j}^2} dk,\end{aligned}\quad (26)$$

where $M_{\text{eff}} = M - g_\sigma s$ denotes the effective nucleon mass and $n_{3b} = \langle \bar{\psi} \gamma^0 \tau_3 \psi \rangle = n_p - n_n$, and g under the sum represents the number of degrees of freedom. The nonlinear meson interaction terms which are necessary for the construction of a correct nuclear matter EoS alter both the isoscalar and isovector sectors [31,48]. However, since the expectation value of the ρ field is generally an order of magnitude smaller than that of the ω field, higher-order nonlinear couplings of the ρ meson are not considered because they only have a marginally influence on the properties of finite nuclei. In the case of infinite nuclear matter, it was shown that the quartic ρ meson coupling gives a measurable effect only in stars made of pure neutron matter. As an example of the parametrization that considers the quartic ρ meson term, the results obtained in Ref. [49] can be given. This paper analyzes the relationship between the skin of heavy nuclei rich in neutrons and the properties of a neutron-star crust. It was verified that changes in parameter sets that lead to an increase in the effective mass of the nucleon or increase the strength of the ρ meson coupling lead to the softening of the EoS for high densities, which gives as a result neutron-star models with slightly smaller radii. The appropriate coupling constants determine the strength of the nonlinear meson interactions. The energy density of the system given by Eq. (26) encodes the correct form of the symmetry energy. The Taylor series expansion method is a simple and generally accepted approximation that makes it possible to calculate its density dependence. The following equations present the explicit form of the symmetry energy $E_{\text{sym},2}(n_b)$ and its slope

TABLE I. Parameters characterizing isospin asymmetric nuclear matter that are subject to experimental constraints.

Coefficient	Span of experimental constraints
$E_{\text{sym},2}(n_0)$	25–35 MeV
$E_{\text{sym},2}(n_0)$	30–35 MeV
L_0	25–115 MeV
$K_{\tau,v}^0(n_0)$	−700– −400 MeV
$\frac{E_{\text{sym},2}(n_0/2)}{E_{\text{sym},2}(n_0)}$	0.57–0.86

$L(n_b)$:

$$\begin{aligned}E_{\text{sym},2}(n_b) &= \frac{k_F^2}{6\sqrt{k_F^2 + M_{\text{eff}}^2}} + \frac{g_\rho^2 n_b}{8m_{\rho,\text{eff}}^2}, \\ L(n_b) &= \frac{k_F^2}{3\sqrt{k_F^2 + M_{\text{eff}}^2}} - \frac{k_F^4}{6\sqrt{(k_F^2 + M_{\text{eff}}^2)^3}} \\ &\quad \times \left(1 + \frac{2M_{\text{eff}} k_F}{\pi^2} \frac{\partial M_{\text{eff}}}{\partial n_b} \right) + \frac{3g_\rho^2}{8m_{\rho,\text{eff}}^2} n_b \\ &\quad - \frac{3g_\rho^2}{8m_{\rho,\text{eff}}^4} \frac{\partial m_{\rho,\text{eff}}^2}{\partial n_b} n_b^2,\end{aligned}\quad (27)$$

where $m_{\rho,\text{eff}}^2 = m_\rho^2 + g_\sigma s g_\rho^2 (2\alpha_2 + \alpha'_2 g_\sigma s) + \alpha'_3 (g_\omega g_\rho)^2 \omega_0^2$ denotes the effective mass of the ρ meson. The first component of the sum in the symmetry-energy expression, Eq. (27), is the kinetic part and the second represents the potential-energy contribution.

Parameters

The process of a continuous and more accurate description of the properties of nuclear matter requires using reliable models. In the case of RMF models, it consists of the appropriate selection of model parameters. The presented discussion is based on the calculations performed using selected models, the parametrizations of which are studied in Refs. [13,50]. Their compliance with the limitations resulting from the analysis of experimental data obtained for nuclear matter with different values of isospin asymmetry, emphasizing the necessity to reproduce the properties of symmetric matter and neutron matter, justifies this choice. The choice of experimental constraints in the case of symmetrical matter ($\delta = 0$) considers the nuclear matter incompressibility at saturation density K_0 in the range 190–270 MeV [51–53], the skewness coefficient $-Q$ in the range 200–1200 MeV [54], the pressure $P(n_b)$ in density ranges $(2n_0, 5n_0)$ and $(1.5n_0, 2.5n_0)$ [2,55]. The last group of limitations is addressed to the isovector sector of the EoS [35], and more specifically to the symmetry energy coefficient $E_{\text{sym}}(n_0)$ [56], the symmetry energy slope L_0 evaluated at n_0 [57,58], the volume part of the isospin incompressibility $K_{\tau,v}^0$ at n_0 [13,59,60], and the ratio of the symmetry energy at $n_0/2$ to its value at n_0 [61]. Individual values of constraints for the coefficients characterizing the isospin-dependent part of the EoS are summarized in Table I. Thus, the carefully selected sets of parameters that

satisfactorily meet the nuclear matter constraints were used for the analysis in this paper. A characteristic feature of the selected models is the variety of nonlinear meson interaction terms. Their presence in the isospin-dependent sector makes it possible to remodel the density dependence of the symmetry energy.

IV. TWO-DIMENSIONAL REGRESSION FOR THE $L_0/E_{\text{sym},2}(n_0)$ RATIO

The function $r^*(n_b)$, Eq. (19), which represents approximate form of the specific parabolic approximation $r(n_b)$ includes, in the exponent, the term $L_0/E_{\text{sym},2}(n_0)$. This factor originates from the parabolic approximation and suggests that the ratio $\frac{L_0}{E_{\text{sym},2}(n_0)}$ is worth attention. It can be recast to the following form:

$$\frac{L_0}{E_{\text{sym},2}(n_0)} = \frac{L_0^{\text{kin}}}{E_{\text{sym},2}(n_0)} + \frac{L_0^{\text{pot}}}{E_{\text{sym},2}(n_0)}, \quad (29)$$

where $L_0 = L_0^{\text{kin}} + L_0^{\text{pot}}$ is decomposed into the kinetic and potential parts, respectively. The power-law relation for the density dependence of the symmetry energy introduces the factor γ , Eq. (9), that differentiates the considered models and can be expressed as follows:

$$\gamma = \frac{L_0^{\text{pot}}}{3E_{\text{sym},2}^{\text{pot}}(n_0)}. \quad (30)$$

The potential part of the symmetry energy can be given by the formula [see Eq. (27)]

$$E_{\text{sym},2}^{\text{pot}}(n_b) = \frac{g_\rho^2 n_b}{8m_{\rho,\text{eff}}^2}, \quad (31)$$

and, in such case, the kinetic energy has the form

$$E_{\text{sym},2}^{\text{kin}} = \frac{k_F^2}{6\sqrt{k_F^2 + M_{\text{eff}}^2}}. \quad (32)$$

The exponent in the power-law parametrization of the symmetry energy corresponding to the division of the symmetry energy into the potential and kinetic part given by Eqs. (31) and (32) is denoted by γ_1 . A second parameter γ_2 [50], which corresponds to the modified form of the potential symmetry energy, could be used. It is related to the splitting of the symmetry energy into kinetic and potential parts. In the case of γ_2 , the kinetic part does not include the medium-modified effective nucleon mass and is given by the formula

$$E_{\text{sym},2}^{\text{kin}} = \frac{k_F^2}{6\sqrt{k_F^2 + M^2}}, \quad (33)$$

the potential symmetry energy is also remodeled

$$E_{\text{sym},2}^{\text{pot}} = \frac{k_F^2}{6\sqrt{k_F^2 + M_{\text{eff}}^2}} - \frac{k_F^2}{6\sqrt{k_F^2 + M^2}} + \frac{g_\rho^2 n_b}{8m_{\rho,\text{eff}}^2}. \quad (34)$$

The changed symmetry energy distribution causes a correspondingly changed distribution of its slope. So there is a possibility to include the power-law parametrization in the

performed analysis. Using Eq. (30) the ratio $L_0/E_{\text{sym},2}(n_0)$ can be rewritten as

$$\frac{L_0}{E_{\text{sym},2}(n_0)} = 1 \frac{L_0^{\text{kin}}}{E_{\text{sym},2}(n_0)} + \left(3 \frac{E_{\text{sym},2}^{\text{pot}}(n_0)}{E_{\text{sym},2}(n_0)} \right) \gamma, \quad (35)$$

or

$$\frac{L_0}{E_{\text{sym},2}(n_0)} = \left(\frac{E_{\text{sym},2}^{\text{kin}}(n_0)}{E_{\text{sym},2}(n_0)} \right) \frac{L_0^{\text{kin}}}{E_{\text{sym},2}^{\text{kin}}(n_0)} + \left(3 \frac{E_{\text{sym},2}^{\text{pot}}(n_0)}{E_{\text{sym},2}(n_0)} \right) \gamma, \quad (36)$$

where the almost constancy of the factor $3E_{\text{sym},2}^{\text{pot}}(n_0)/E_{\text{sym},2}(n_0)$ across the RMF models, [13], is the reason for the decompositions (35) or (36) with γ being as one of the two variables on the RHS of these equations. In this way, γ naturally appears in the analysis. It will be checked that the variability of $E_{\text{sym},2}^{\text{kin}}(n_0)/E_{\text{sym},2}(n_0)$ in Eq. (36) is also negligible, allowing for treating its mean across the RFM models as a coefficient before the variable $L_0^{\text{kin}}/E_{\text{sym},2}^{\text{kin}}(n_0)$ (see Secs. IV B 1 and IV B 2). In the analysis of models (35) and (36), the Akaike information criterion is used for model selection [69]. The motivation behind its usage is the maximum likelihood method, which maximizes the probability of realization of the observed sample, in this case, represented by the analyzed set of models. This will be explained in Sec. IV A. In Sec. IV B, it will be shown that, by using the Akaike information criterion, the discussed representations (35) and (36) of $L_0/E_{\text{sym},2}(n_0)$ enables one to differentiate between various forms of the kinetic part of the symmetry energy. This distinction is based on the fact that if the kinetic energy is given by the formula (33), then the Akaike criterion picks out the model (36), with $E_{\text{sym},2}^{\text{kin}}(n_0)$ in the denominator of the first factor. Contrary to this, when the kinetic energy takes into account the effective mass of the nucleon, Eq. (32), the model (35) is preferred, with $E_{\text{sym},2}(n_0)$ in the denominator of the first factor. Application of the Akaike criterion to this problem requires the construction of appropriate regression functions related to the pair of relationships (35) and (36), and the assumption that the variable $L_0/E_{\text{sym},2}(n_0)$ and the factors $L_0^{\text{kin}}/E_{\text{sym},2}(n_0)$ and γ in Eq. (35) or $L_0^{\text{kin}}/E_{\text{sym},2}^{\text{kin}}(n_0)$ and γ in Eq. (36) are random variables. Although analytical models (35) and (36) are equivalent, they lead to different linear regression models in the population of all considered models. That is, when $L_0/E_{\text{sym},2}(n_0)$ is treated as the response variable and the factors $L_0^{\text{kin}}/E_{\text{sym},2}(n_0)$ and γ in Eq. (35) or the factors $\frac{L_0^{\text{kin}}}{E_{\text{sym},2}^{\text{kin}}(n_0)}$ and γ in Eq. (36) are recognized as the explanatory ones then Eq. (35) and Eq. (36) can be perceived as two regression models in the space of the discussed models. Due to the difference in the form of the factor $L_0^{\text{kin}}/E_{\text{sym},2}(n_0)$ in Eq. (35) and $L_0^{\text{kin}}/E_{\text{sym},2}^{\text{kin}}(n_0)$ in Eq. (36), the matching of these two regression models to the sample of the considered models in which the kinetic term is constructed differently, will also be different. An additional reason for such a choice of factors is that the coefficients standing before them have relatively

low variability in the group of the studied RMF models (see Secs. IV B 1 and IV B 2).

From the analytical models given by Eqs. (35) and (36) it is evident that the intercept is equal to zero. Thus, the form of the analytical models (35) and (36) requires that the intercept (offset) in the statistical counterparts of these equations is also equal to zero. Therefore, two statistical regression models f_k , $k = 1, 2$ (see Sec. IV B), are proposed:

$$\text{Model}_1 : \frac{L_0}{E_{\text{sym},2}(n_0)} = \alpha_{1,1} \frac{L_0^{\text{kin}}}{E_{\text{sym},2}(n_0)} + \alpha_{1,2}\gamma + E, \quad (37)$$

where $L_0/E_{\text{sym},2}(n_0)$ is the response, and $L_0^{\text{kin}}/E_{\text{sym},2}(n_0)$ and γ are the factors and E is the error (random ingredient), or

$$\text{Model}_2 : \frac{L_0}{E_{\text{sym},2}(n_0)} = \alpha_{2,1} \frac{L_0^{\text{kin}}}{E_{\text{sym},2}^{\text{kin}}(n_0)} + \alpha_{2,2}\gamma + E, \quad (38)$$

where $L_0/E_{\text{sym},2}(n_0)$ is the response, and $L_0^{\text{kin}}/E_{\text{sym},2}^{\text{kin}}(n_0)$ and γ are the factors and E is the error. In a compact form these models can be rewritten as follows:

$$\text{Model}_M : \frac{L_0}{E_{\text{sym},2}(n_0)} = \left(\frac{L_0}{E_{\text{sym},2}(n_0)} \right)_{\text{theor}} + E, \quad (39)$$

where $[L_0/E_{\text{sym},2}(n_0)]_{\text{theor}}$ is the theoretical (theor) value (the conditional expectation value) of the response, i.e.,

$$\left(\frac{L_0}{E_{\text{sym},2}(n_0)} \right)_{\text{theor}} = \alpha_{M,1}A_M + \alpha_{M,2}\gamma. \quad (40)$$

Here, for $M = 1$ the corresponding statistical model is called f_1 with the first factor $A_M = A_1 = L_0^{\text{kin}}/E_{\text{sym},2}(n_0)$, and for $M = 2$ the corresponding statistical model is called f_2 with the first factor $A_M = A_2 = L_0^{\text{kin}}/E_{\text{sym},2}^{\text{kin}}(n_0)$.

If a sample of N models is chosen from the population of RMF models, then the regression model (40) is estimated by

$$\frac{L_0}{E_{\text{sym},2}(n_0)} = \frac{\widehat{L_0}}{E_{\text{sym},2}(n_0)} + \hat{E}, \quad (41)$$

where

$$\frac{\widehat{L_0}}{E_{\text{sym},2}(n_0)} = \hat{\alpha}_{M,1}A_M + \hat{\alpha}_{M,2}\gamma \quad (42)$$

is the conditional mean of the response and the error term E in Eq. (39) is replaced by its estimate \hat{E} . Throughout this paper, the variance of the error term \hat{E} is denoted by MSE (mean squared error) [70].

A. The consistency assumption for every relativistic mean-field model

In this paper, it is assumed that every theoretical RMF point in the sample of $N = 23$ RMF models is estimated consistently (and thus without any bias, at least asymptotically). Therefore, every theoretical RMF point on the scatter diagram [with coordinates $L_0/E_{\text{sym},2}(n_0)$ for the response and A_M and γ for the factors] coincides with the estimate obtained for the infinite number n of hypothetical experiments testing this RMF model. It follows that in the limits $n \rightarrow \infty$ and for all the population of RMF models, the finite sample error \hat{E} tends to E .

B. The Akaike information criterion analysis

Below, the Akaike information criterion model selection procedure for the ($N = 23$) RMF model points is used. In Secs. IV B 1 and IV B 2 the estimation of regression models (37) and (38) using the sample of $N = 23$ points of the RMF models is performed.

To select the better regression model from the two models (37) and (38) considered in this paper, the Akaike information criterion for the normal distribution of the response $L_0/E_{\text{sym},2}(n_0)$ and explanatory variables A_M and γ is used. The Akaike information criterion (AIC) for a model with a “free” parameter Θ_K is defined as follows:

$$AIC(\Theta_K) = -2 \ln L(\hat{\Theta}_K) + 2K, \quad (43)$$

where $L(\Theta_K)$ is the likelihood function of the model with Θ_K parameter in the N -dimensional sample and $\hat{\Theta}_K$ is a maximum likelihood (ML) estimator of the K -dimensional parameter Θ_K . In Sec. IV, $\Theta_{K=2} = (\alpha_{1,1}, \alpha_{1,2})$ for Model₁ and $\Theta_{K=2} = (\alpha_{2,1}, \alpha_{2,2})$ for Model₂. More information on the Akaike information criterion model selection can be found, e.g., in Ref. [69]. In the sense of Kullback-Leibler relative entropy, a model with a lower value of AIC can be understood as being closer than other models to a certain “true” model. This can be justified in the following way: Let the data $y = (y_1, y_2, \dots, y_N)$ be generated by the unknown, true model g for the random variable Y and let the model f_k be the candidate for the description of the investigated phenomenon (e.g., the statistical models f_1 for the regression Model₁ and f_2 for the regression Model₂, see Sec. IV). Thus, the model $f_k \equiv f_k(Y, \Theta_K)$ in the light of data coming from the $g(Y)$ model is considered. The maximization of the log-likelihood function $\ln L_f(y|\Theta_K)$ for L_f being the likelihood function for the f_k model is asymptotically (or on average) equivalent to maximizing the expectation value

$$\lambda(\Theta_K) \equiv E_g[\ln f_k(Y, \Theta_K)].$$

The parameter Θ_K is unknown, thus, it is replaced by its maximum likelihood method (MLM) estimator $\hat{\Theta}_K$. Therefore, instead of $\lambda(\Theta_K)$ the expectation value

$$Q_K \equiv E_{g, h_{\Theta_K}}[\ln f_k(Y, \hat{\Theta}_K)]$$

is maximized, where h_{Θ_K} is the distribution $h_{\Theta_K}(\hat{\Theta}_K)$ of the estimator $\hat{\Theta}_K$. The maximization of Q_K is equivalent to the minimization of $-2NQ_K$, where N is the dimension of the sample. As $AIC(f_k)$ is approximately the unbiased estimator of $-2NQ_K$, the model which minimizes $AIC(f_k)$ is chosen. Asymptotically (or in the mean), the MLM is equivalent to the minimization of the Kullback-Leibler distance

$$\begin{aligned} D(g, f) &= E_g[\ln g(Y)] - E_g[\ln f_k(Y, \Theta_K)] \\ &= E_g[\ln g(Y)] - \lambda(\Theta_K) \end{aligned} \quad (44)$$

between the models f_k and g . In this case, the minimization of $AIC(f_k)$ implies the selection of the model that minimizes the distance of the model f_k chosen for the purpose of the statistical analysis from the unknown, true model g .

TABLE II. The characteristics of the two-dimensional linear regressions $Y \equiv L_0/E_{\text{sym},2}(n_0) = \hat{\alpha}_{M,1}A_M + \hat{\alpha}_{M,2}\gamma + \hat{E}$, $M = 1, 2$, (41), (42) for γ_1 and γ_2 , where $A_1 = L_0^{\text{kin}}/E_{\text{sym},2}(n_0)$, $A_2 = L_0^{\text{kin}}/E_{\text{sym},2}^{\text{kin}}(n_0)$ and $n_b = n_0$. The characteristics of the regressions are the Akaike information criterion AIC for the model defined in Eq. (43) and supplementarily, the mean square due to regression MSR [70], the mean squared error MSE (which is the variance of the error term \hat{E}), and the coefficient of determination $R^2 = SSR/SSY$, where SSR and SSY are the sum of squares due to regression and the total sum of squares of the response Y , respectively, and $SSY = SSR + SSE$, where SSE is the error sum of squares. The values of $\hat{\alpha}_{M,1}$, $\hat{\alpha}_{M,2}$ are the estimates of the structural parameters of a particular regression model and \hat{Y} stands for the approximant of $Y_{\text{theor}} = \alpha_{M,1}A_M + \alpha_{M,2}\gamma$. $\hat{\sigma}_{\hat{\alpha}_{M,1}}$ and $\hat{\sigma}_{\hat{\alpha}_{M,2}}$ are the standard errors of $\hat{\alpha}_{M,1}$ and $\hat{\alpha}_{M,2}$, respectively. The regression model does not contain an offset.

$\hat{Y} = \hat{\alpha}_{M,1}A_M + \hat{\alpha}_{M,2}\gamma$		$\hat{\alpha}_{M,1}$	$\hat{\sigma}_{\hat{\alpha}_{M,1}}$	$\hat{\alpha}_{M,2}$	$\hat{\sigma}_{\hat{\alpha}_{M,2}}$	AIC	SSE	MSR	MSE	R^2	N
$\hat{Y} = \hat{\alpha}_{1,1}A_1 + \hat{\alpha}_{1,2}\gamma$, $\gamma = \gamma_1$		0.98417	0.01223	1.49976	0.04164	-75.32436	0.0426263	50.13187	0.00203	0.9996	23
$\hat{Y} = \hat{\alpha}_{2,1}A_2 + \hat{\alpha}_{2,2}\gamma$, $\gamma = \gamma_1$		0.56087	0.00739	1.21478	0.04744	-72.61983	0.0479453	50.12921	0.00228	0.9995	23
$\hat{Y} = \hat{\alpha}_{1,1}A_1 + \hat{\alpha}_{1,2}\gamma$, $\gamma = \gamma_2$		0.89957	0.03121	2.05395	0.02891	-107.85549	0.0103613	50.14800	0.00049339	0.9999	23
$\hat{Y} = \hat{\alpha}_{2,1}A_2 + \hat{\alpha}_{2,2}\gamma$, $\gamma = \gamma_2$		0.34671	0.00441	1.96486	0.01171	-153.54415	0.0014214	50.15247	0.00006768	≈ 1	23

1. Model selection for $\gamma \equiv \gamma_1$

The analysis of the sample of $N = 23$ models for $\gamma \equiv \gamma_1$ (Table II) gives $AIC(\text{Model}_1) = -75.32436$ and $AIC(\text{Model}_2) = -72.61983$. As $AIC(\text{Model}_1) < AIC(\text{Model}_2)$, therefore Model_1 is chosen, for which $A_M = A_1 = L_0^{\text{kin}}/E_{\text{sym},2}(n_0)$. Then the estimates of the structure parameters $\alpha_{1,1}$ and $\alpha_{1,2}$ are

$$\text{Model}_1 : \hat{\alpha}_{1,1} = 0.98417 \text{ and } \hat{\alpha}_{1,2} = 1.49976, \quad (45)$$

and the N sample estimate of $[L_0/E_{\text{sym},2}(n_0)]_{\text{theor}}$, Eq. (42), is

$$\frac{\widehat{L_0}}{E_{\text{sym},2}(n_0)} = \hat{\alpha}_{1,1} \frac{L_0^{\text{kin}}}{E_{\text{sym},2}(n_0)} + \hat{\alpha}_{1,2}\gamma. \quad (46)$$

Here,

$$\frac{\widehat{L_0}}{E_{\text{sym},2}(n_0)}$$

is the conditional mean of $L_0/E_{\text{sym},2}(n_0)$.

The scatter plot of the RMF models and the regression surface given by Eq. (46) is shown in Fig. 1. If the considered RMF points exhaust all physical situations, then $\hat{\alpha}_{1,1} = \alpha_{1,1}$

and $\hat{\alpha}_{1,2} = \alpha_{1,2}$. For the considered sample of $N = 23$ RMF models for $\gamma = \gamma_1$, the relative standard errors of estimation of $\alpha_{1,1}$ and $\alpha_{1,2}$ are equal to 1.243% and 2.776%, respectively (see Table II). The coefficient of determination R-squared [70], which is a goodness-of-fit measure for linear regression models, has the value $R^2 = 0.9996$ (see Table II). The corresponding means $\bar{1} = 1$ and

$$3 \frac{\overline{E_{\text{sym},2}^{\text{pot}}(n_0)}}{E_{\text{sym},2}(n_0)} = 1.42496$$

[see Eq. (35)] are close to the values $\hat{\alpha}_{1,1} = 0.98417$ and $\hat{\alpha}_{1,2} = 1.49976$, respectively. This fact, together with the weak variability of $3E_{\text{sym},2}^{\text{pot}}(n_0)/E_{\text{sym},2}(n_0)$, for which the coefficient of variation $V[3E_{\text{sym},2}^{\text{pot}}(n_0)/E_{\text{sym},2}(n_0)] = 8.601\%$, justifies the assumption that the factors on the right-hand side (RHS) of Eq. (35) are $L_0^{\text{kin}}/E_{\text{sym},2}(n_0)$ and γ . Nevertheless, this weak variability of $3E_{\text{sym},2}^{\text{pot}}(n_0)/E_{\text{sym},2}(n_0)$, suggests that the coefficients 1 and $3E_{\text{sym},2}^{\text{pot}}(n_0)/E_{\text{sym},2}(n_0)$ in Eq. (35) have to be replaced by ones resulting from the correction of the relation (30). This could follow from taking into account the higher-order terms in Eq. (5).

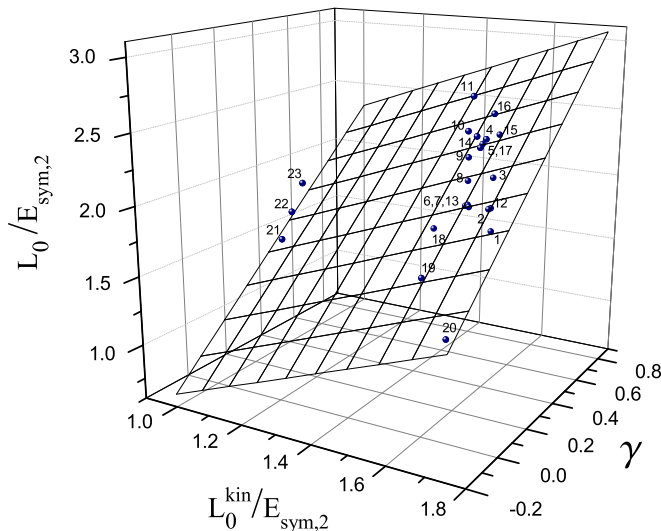


FIG. 1. Plot of the two-dimensional regression surface for γ_1 . The RMF models are numbered in the order they appear in Table II.

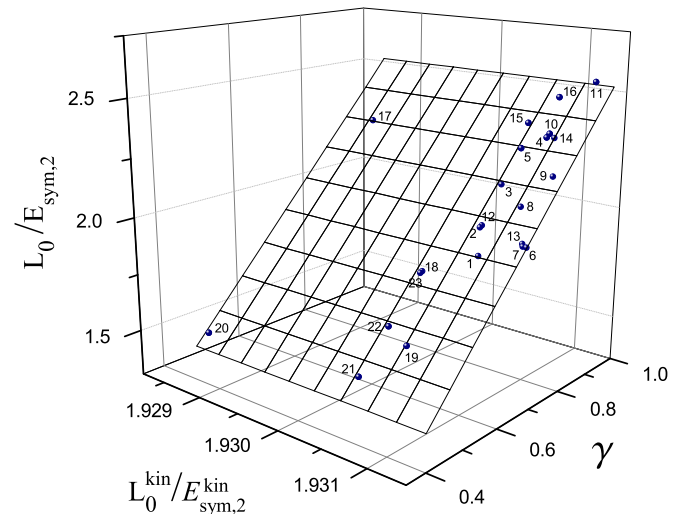


FIG. 2. Plot of the two-dimensional regression surface for γ_2 . The RMF models are numbered in the order they appear in Table II.

TABLE III. An exemplary characteristic of models in terms of the nonlinear couplings of mesons.

Group	Models	$\sigma - \omega^2$	$\sigma^2 - \omega^2$	$\sigma - \rho^2$	$\sigma^2 - \rho^2$	$\rho^2 - \omega^2$	$m_{\rho,\text{eff}}^2$
Group Ia	BSR	+	+	+	+	+	$m_{\rho}^2 + g_{\sigma} s g_{\rho}^2 (2\alpha_2 + \alpha_2' g_{\sigma} s) + \alpha_3' (g_{\omega} g_{\rho})^2 \omega_0^2$
	FSUGZ03	+	+	+	+	+	
	FSUGZ06	+	+	+	+	+	
Group Ib	BKA	+	+	+	-	-	$m_{\rho}^2 + 2\alpha_2 g_{\sigma} g_{\rho}^2 s$
	G2*	+	+	+	-	-	
Group II	FSUGold	-	-	-	-	+	$m_{\rho}^2 + \alpha_3' (g_{\omega} g_{\rho})^2 \omega_0^2$
	FSUGold4	-	-	-	-	+	
	IU-FSU	-	-	-	-	+	
Group III	Z271s6	-	-	-	+	-	$m_{\rho}^2 + \alpha_2' (g_{\sigma} g_{\rho})^2 s^2$
	Z271s5	-	-	-	+	-	
	Z271s4	-	-	-	+	-	

2. Model selection for $\gamma \equiv \gamma_2$

Similarly, the analysis of the sample of $N = 23$ models for $\gamma \equiv \gamma_2$ (Table II) gives $AIC(\text{Model}_1) = -107.85549$ and $AIC(\text{Model}_2) = -153.54415$. As $AIC(\text{Model}_2) < AIC(\text{Model}_1)$, Model_2 is selected, for which $A_M = A_2 = L_0^{\text{kin}}/E_{\text{sym},2}^{\text{kin}}(n_0)$. Then the estimates of the structure parameters $\alpha_{2,1}$ and $\alpha_{2,2}$ are

$$\text{Model}_2 : \hat{\alpha}_{2,1} = 0.34671 \text{ and } \hat{\alpha}_{2,2} = 1.96486, \quad (47)$$

and the N sample estimates of $[L_0/E_{\text{sym},2}(n_0)]_{\text{theor}}$ is

$$\frac{\widehat{L_0}}{E_{\text{sym},2}(n_0)} = \hat{\alpha}_{2,1} \frac{L_0^{\text{kin}}}{E_{\text{sym},2}^{\text{kin}}(n_0)} + \hat{\alpha}_{2,2} \gamma. \quad (48)$$

The corresponding scatter plot of the RMF models and the regression surface given by Eq. (48) is shown in Fig. 2. If the considered RMF points exhaust all physical situations then $\hat{\alpha}_{2,1} = \alpha_{2,1}$ and $\hat{\alpha}_{2,2} = \alpha_{2,2}$. For the considered sample of $N = 23$ RMF models for $\gamma = \gamma_2$, the relative standard errors of

estimation of $\alpha_{2,1}$ and $\alpha_{2,2}$ are equal to 1.272% and 0.596%, respectively (see Table II). The coefficient of determination R-squared has the value $R^2 \approx 1$. The means

$$\frac{\overline{E_{\text{sym},2}^{\text{kin}}(n_0)}}{E_{\text{sym},2}(n_0)} = 0.34853$$

and

$$3 \frac{\overline{E_{\text{sym},2}^{\text{pot}}(n_0)}}{E_{\text{sym},2}(n_0)} = 1.95442$$

[see Eq. (36)] are close to the values $\hat{\alpha}_{2,1} = 0.34671$ and $\hat{\alpha}_{2,2} = 1.96486$, respectively. This fact, together with the weak variability of $E_{\text{sym},2}^{\text{kin}}(n_0)/E_{\text{sym},2}(n_0)$ and $3E_{\text{sym},2}^{\text{pot}}(n_0)/E_{\text{sym},2}(n_0)$, for which the coefficient of variation is equal to $V[E_{\text{sym},2}^{\text{kin}}(n_0)/E_{\text{sym},2}(n_0)] = 4.036\%$ and $V[3E_{\text{sym},2}^{\text{pot}}(n_0)/E_{\text{sym},2}(n_0)] = 2.159\%$, respectively, justifies the assumption that the factors on the RHS of Eq. (36)

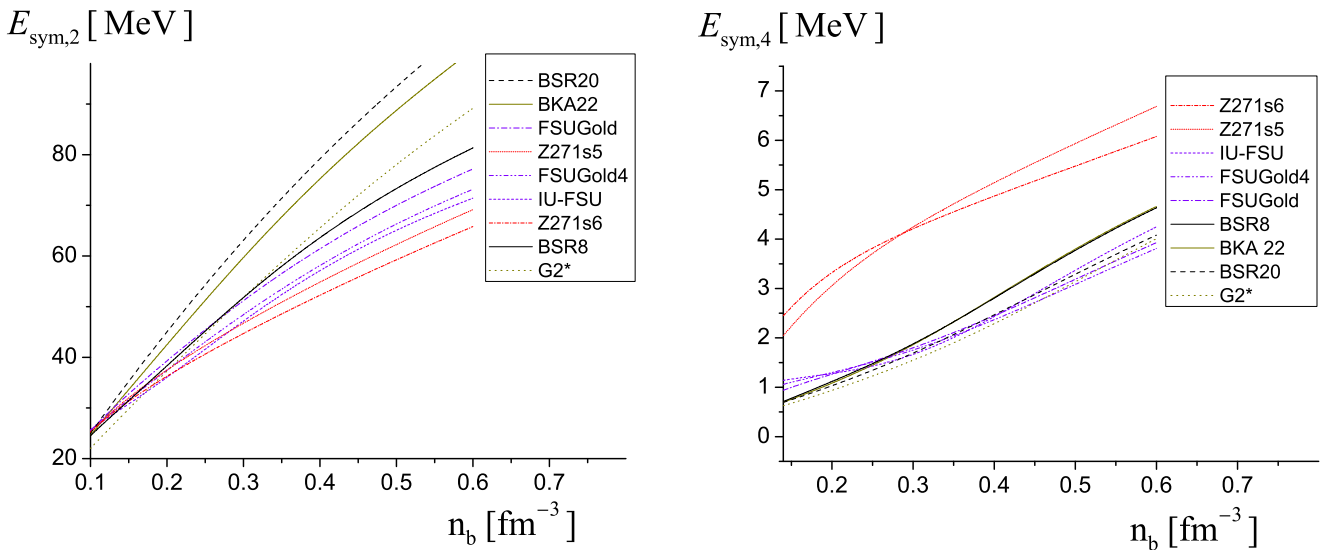


FIG. 3. The left panel shows the density dependence of the symmetry energy $E_{\text{sym},2}(n_b)$ obtained within the parabolic approximation for parametrizations that represent the four groups of models discussed. The right panel depicts the density dependence of the fourth-order symmetry energy $E_{\text{sym},4}(n_b)$. The models are listed in the figure legend according to the dependent variable value (from the lowest to the highest) at the saturation density n_0 of the given model. The same order is also used in other figures where the dependence on n_b is considered.

TABLE IV. Parameters that enter the Lagrange function given by Eq. (24). The mass of the scalar meson m_σ is given in MeV, the parameters A , α_1 , α_2 are given in fm^{-1} .

PS	m_σ	A	B	C	g_σ	g_ω	g_ρ	α_1	α'_1	α_2	α'_2	α'_3
BSR8 [62]	506.51	8.2924	12.4514	0.005	10.6289	13.6599	14.9908	0.0000366	0.0002717	0.0289393	0.0159659	0.0152088
BSR9	500.51	9.72502	21.8004	0.005	10.76147	14.11102	14.67414	0.0010311	0.0005071	0.0306821	0.0116255	0.0135981
BSR10	499.53	10.0262	14.2496	0.005	10.73005	14.04275	13.69014	0.0008281	0.000298	0.031822	0.004754	0.0097721
BSR11	497.21	9.96589	23.3484	0.005	10.71942	14.12534	12.19156	0.001065	0.0006526	0.0277742	0.0022126	0.0045581
BSR12	499.12	10.6055	10.2259	0.005	10.61808	13.88708	10.96456	0.001259	0.0000052	0.01187	0.01276	0.002898
BSR15	503.44	4.4934	61.2708	0.01	11.05170	14.65579	14.98725	0.0000601	0.0000203	0.0286236	0.0155176	0.0155307
BSR16	501.37	4.4934	61.2708	0.01	11.02412	14.66595	14.52186	0.0000449	0.0000526	0.0258355	0.0156881	0.0158487
BSR17	499.38	5.05566	57.9698	0.01	10.95765	14.59582	13.41111	0.0000409	0.0001079	0.0266308	0.0130876	0.0084916
BSR18	497.27	5.21809	60.7499	0.01	11.01908	14.77458	11.94837	0.0001469	0.0001559	0.0202292	0.0090169	0.0096305
BSR19	495.82	5.87325	55.2713	0.01	10.91944	14.64700	10.71055	0.0003499	0.000023	0.0124695	0.0077919	0.0074863
BSR20	490.83	7.76788	63.7487	0.01	11.10806	15.19792	10.08835	0.0014153	8.5×10^{-6}	0.0118538	0.0027422	0.0040699
FSUGZ03 [63]	500.511	9.7247	21.8007	0.005	10.76145	14.11104	14.67414	0.001031	0.000507	0.030682	0.011625	0.013598
FSUGZ06	501.370	4.6551	60.2782	0.01	11.02412	14.66595	14.52185	0.000045	0.000053	0.025836	0.015688	0.015849
BKA20 [64]	509.90	8.16.93	9.992	0.806	10.11	12.69	12.32	0.00107	0.00015	0.0019		
BKA22	497.86	11.0243	11.31	0.97	10.63	13.93	12.95	0.00028	0.00012	0.00788		
BKA24	509.88	12.5379	16.63	1.038	10.80	14.40	11.79	0.000451	0.000194	0.004158		
G2* [65]	520.206	5.2284	3.5594	0.0027	10.4929	12.7676	11.7873	0.00658	0.000234	0.0517		0.06
FSUGold [31]	519.194	4.2744	49.8099	0.01	10.5924	14.302	11.7673					0.08
FSUGold4 [66]	519.194	4.2744	49.8099	0.01	10.5924	14.302	13.5138					0.02
IU-FSU [67]	491.500	8.4928	0.4877	0.005	9.9713	13.0321	13.590					
Z272s6[68]	465.0	5.4345	63.6911	0.01	7.0314	8.4065	12.1119				0.12	
Z272s5	465.0	5.4345	63.6911	0.01	7.0314	8.4065	11.5254				0.1	
Z272s4	465.0	5.4345	63.6911	0.01	7.0314	8.4065	11.0167				0.08	

TABLE V. The characteristics of $Y \equiv E_{\text{sym},2}(n_0)$ vs $X \equiv L_0$ regression: the mean square due to regression MSR , the mean squared error MSE and the coefficient of determination R^2 . When the error sum of squares $SSE = 0$ then the total mean square MSY for the response Y is given, a , b and c are the estimates of the structural parameters of a particular regression model. In the linear regression case $c = 0$. N_i is the size of the group.

	a	b	c	MSR	MSE	R^2	N_i
$\hat{E}_{\text{sym},2} = a + bL_0 + cL_0^2$	MeV		MeV ⁻¹	MeV ²	MeV ²		
Group Ia (BSR, FSUGZ03, FSUGZ06)	11.23958	0.45512	-0.00215	9.36761	0.03115	0.98364	13
Group Ib (BKA, G2*)	-39.04488	1.60742	-0.00877	3.89676	0.00335	0.99957	4
Group II (FSUGold, FSUGold4, IU-FSU)	51.04781	-0.82104	0.00853	MSY = 0.51905		1	3
Group III (Z271s6, Z271s5, Z271s4)	24.46057	0.16761	-5.58035 × 10 ⁻⁴	MSY = 0.44163		1	3
All groups	39.47017	-0.30662	0.0028927	11.16314	0.41083	0.73098	23
$\hat{E}_{\text{sym},2} = a + bL_0$	MeV			MeV ²	MeV ²		
Group Ia (BSR, FSUGZ03, FSUGZ06)	22.47243	0.14171		18.48784	0.050807	0.97066	13
Group Ib (BKA, G2*)	13.04805	0.25223		7.57194	0.11247	0.97115	4
Group II (FSUGold, FSUGold4, IU-FSU)	26.30182	0.10275		0.96372	0.07439	0.92834	3
Group III (Z271s6, Z271s5, Z271s4)	26.0775	0.10727		0.88295	0.00030125	0.99966	3
All groups	26.8095	0.081484		18.86494	0.55609	0.61765	23

are $L_0^{\text{kin}}/E_{\text{sym},2}^{\text{kin}}(n_0)$ and γ . Thus, $E_{\text{sym},2}^{\text{kin}}(n_0)/E_{\text{sym},2}(n_0)$ and $3E_{\text{sym},2}^{\text{pot}}(n_0)/E_{\text{sym},2}(n_0)$ in Eq. (36) are equal to almost constant coefficients. Nevertheless, this weak variability of $E_{\text{sym},2}^{\text{kin}}(n_0)/E_{\text{sym},2}(n_0)$ and $3E_{\text{sym},2}^{\text{pot}}(n_0)/E_{\text{sym},2}(n_0)$ suggests that the coefficients $E_{\text{sym},2}^{\text{kin}}(n_0)/E_{\text{sym},2}(n_0)$ and $3E_{\text{sym},2}^{\text{pot}}(n_0)/E_{\text{sym},2}(n_0)$ in Eq. (36) have to be replaced by new ones, resulting from correcting the relation Eq. (30). This could be acquired by taking into account higher-order terms in Eq. (5).

V. RESULTS

The assumption that every theoretical RMF point in the sample of $N = 23$ models is estimated consistently was adopted for all regression analyses. From Secs. IV B 1 and IV B 2 it follows that the symmetry energy decomposition into the kinetic and potential parts is reflected in the results obtained by the Akaike information criterion for model selection (Table II). For the reason that there are differences in the form of the first factors $A_1 = L_0^{\text{kin}}/E_{\text{sym},2}(n_0)$ in Eq. (35) and $A_2 = L_0^{\text{kin}}/E_{\text{sym},2}^{\text{kin}}(n_0)$ in Eq. (36), the fits of these two regression models to the sample of models considered, in which the kinetic component is constructed differently, are also different. In the first case, the Akaike criterion chooses the model described by Eq. (35). Therefore, the exponent in the power-law parametrization of the potential part of the symmetry energy, Eq. (8), is given by γ_1 , whereas for the factor constructed from the pure kinetic terms only [i.e., $L_0^{\text{kin}}/E_{\text{sym},2}^{\text{kin}}(n_0)$] the model specified by Eq. (36) with the exponent γ_2 is preferred. Thus, when applied to the power-law shape of the symmetry energy, the two-dimensional regression model analysis leads to density dependence of the symmetry energy differentiated by the value of the γ exponent.

Next, a one-dimensional regression analysis was performed to provide supplementary information about the sample of selected models. Due to the ρ meson effective mass, all models in the considered sample are divided into four groups. Details are given in Tables III and IV. Underneath

these groups reveal themselves in one-dimensional regression analysis between the input parameters. The assumption was made that the theoretical value of a response Y , i.e., the conditional expectation value, is $Y_{\text{theor}} = \alpha + \beta X$, where X is a factor. Then the estimator of Y_{theor} in the sample of N models is the conditional mean $\hat{Y} = \hat{\alpha} + \hat{\beta}X$, where $\hat{\alpha}$ and $\hat{\beta}$ are the estimators of the structural parameters α and β of the regression model. The values of the estimators $\hat{\alpha}$ and $\hat{\beta}$ in the sample will be denoted by a and b , respectively. The regression model in the sample has the form $Y = \hat{Y} + \hat{E}$, where \hat{E} is the error. The results for analyzed linear regressions between various input parameters X and Y are collected in Tables V–IX. If N considered RMF points would exhaust all physical situations, then the estimates $a = \alpha$ and $b = \beta$.

A. Inaccuracy of the parabolic approximation: The role of the symmetry energy

The input parameters used in the performed regression analysis include, among others, coefficients characterizing the dependence of the symmetry energy on the density. Thus, the second $E_{\text{sym},2}(n_b)$ and fourth-order $E_{\text{sym},4}(n_b)$ symmetry energy functions are the analysis's starting point. Results in the left and right panels in Fig. 3 were obtained for the representative parametrizations for selected groups of models. The division of the considered models into groups will be justified later in the text.

The nonlinear meson interaction terms modify the system's energy density. Such a modification is equivalent to changing the main EoS characteristics, appearing in Taylor expansion for the symmetric and asymmetric matter. In the case of asymmetric matter, these changes concern, among others, the symmetry-energy coefficient, the form of the symmetry energy, and its slope. Providing that the parabolic approximation is sufficient, the symmetry-energy dependencies on density $E_{\text{sym},2}(n_b)$ show behavior characteristic of the RMF models, i.e., they are functions increasing with density. It is well known that an almost linear relationship is obtained in the extreme case, but it can be easily modified by including

TABLE VI. The characteristics of $E_{\text{sym},2}^{-1}(n_0)$ vs L_0 , $E_{\text{sym},2}^{-2}(n_0)$ vs L_0 , $E_{\text{sym},4}(n_0)$ vs L_0 and $E_{\text{sym},4}(n_0)$ vs $E_{\text{sym},2}(n_0)$ regressions. The characteristics of the regressions are the mean square due to regression MSR , the mean squared error MSE and the Pearson correlation coefficient $r_{X,Y}$, a , and b are the estimates of the structural parameters of a particular regression model. N_i is the size of the group. For simplicity, the notation $(\hat{E}_{\text{sym},2}^{-1})^{-1} \equiv \hat{E}_{\text{sym},2}^{-1}$ is used.

RMF Models		a	b	MSR	MSE	Pearson $r_{X,Y}$	N_i
		MeV ⁻¹	MeV ⁻²	MeV ⁻²	MeV ⁻²		
$\hat{E}_{\text{sym},2}^{-1} = a + bL_0$							
Group Ia	BSR, FSUGZ03, FSUGZ06	0.040225	-0.00013302	1.62889×10^{-5}	5.24893×10^{-8}	-0.98273	13
Group Ib	BKA, G2*	0.049504	-0.00024217	6.97979×10^{-6}	1.48663×10^{-7}	-0.97936	4
Group II	FSUGold, FSUGold4, IU-FSU	0.036845	-0.00010067	9.2513×10^{-7}	6.98283×10^{-8}	-0.96427	3
Group III	Z271s6, Z271s5, Z271s4	0.037092	-0.00010566	8.56595×10^{-7}	7.97228×10^{-10}	-0.99953	3
$\hat{E}_{\text{sym},2}^{-2} = a + bL_0$							
Group Ia	BSR, FSUGZ03, FSUGZ06	0.0015281	-8.15952×10^{-6}	6.12898×10^{-8}	2.14622×10^{-10}	-0.98128	13
Group Ib	BKA, G2*	0.0021115	-1.50319×10^{-5}	2.68937×10^{-8}	6.70952×10^{-10}	-0.97595	4
Group II	FSUGold, FSUGold4, IU-FSU	0.0013272	-6.30364×10^{-6}	3.62714×10^{-9}	2.70643×10^{-10}	-0.96466	3
Group III	Z271s6, Z271s5, Z271s4	0.0013436	-6.63339×10^{-6}	3.37631×10^{-9}	4.50592×10^{-12}	-0.99933	3
$\hat{E}_{\text{sym},4} = a + bL_0$							
Group Ia	BSR, FSUGZ03, FSUGZ06	0.81189	-0.00085651	0.00067534	6.03861×10^{-5}	-0.71003	13
Group Ib	BKA, G2*	0.41361	0.0039928	0.0018975	0.00029698	0.87270	4
Group II	FSUGold, FSUGold4, IU-FSU	1.81915	-0.013777	0.017326	0.00030713	-0.99125	3
Group III	Z271s6, Z271s5, Z271s4	5.61190	-0.063199	0.30647	0.00040089	-0.99935	3
$\hat{E}_{\text{sym},4} = a + bE_{\text{sym},2}$							
Group Ia	BSR, FSUGZ03, FSUGZ06	0.9227	-0.0052719	0.00052937	7.36562×10^{-5}	-0.62863	13
Group Ib	BKA, G2*	0.21378	0.015624	0.0019032	0.00029413	0.874	4
Group II	FSUGold, FSUGold4, IU-FSU	4.89437	-0.11987	0.014917	0.0027167	-0.91975	3
Group III	Z271s6, Z271s5, Z271s4	20.98153	-0.58934	0.30677	9.59448×10^{-5}	-0.99984	3

TABLE VII. The characteristics of $w(n_0)$ vs L_0 and $r(n_0)$ vs L_0 regressions. The characteristics of the regressions are the mean square due to regression MSR , the mean squared error MSE , and the Pearson correlation coefficient $r_{x,y}$. a and b are the estimates of the structural parameters of a particular regression model. N_i is the size of the group.

	RMF Models	a	b	MSR	MSE	Pearson $r_{x,y}$	N_i
$\hat{w} = a + bL_0$			MeV^{-1}				
Group Ia	BSR, FSUGZ03, FSUGZ06	0.032046	-0.00012563	1.45281×10^{-5}	3.6959×10^{-8}	-0.9863	13
Group Ib	BKA, G2*	0.026153	-5.10778×10^{-5}	3.10516×10^{-7}	3.04356×10^{-7}	-0.58121	4
Group II	FSUGold, FSUGold4, IU-FSU	0.06296	-0.00053977	2.6595×10^{-5}	9.42149×10^{-8}	-0.99823	3
Group III	Z271s6, Z271s5, Z271s4	0.18889	-0.0022166	0.00037702	8.10382×10^{-7}	-0.99893	3
$\hat{r}_0 = a + bL_0$		MeV^{-1}	MeV^{-2}	MeV^{-2}	MeV^{-2}		
Group Ia	BSR, FSUGZ03, FSUGZ06	0.0012032	-6.90212×10^{-6}	4.38554×10^{-8}	7.93603×10^{-11}	-0.99019	13
Group Ib	BKA, G2*	0.0012255	-7.00547×10^{-6}	5.84109×10^{-9}	4.88933×10^{-10}	-0.92552	4
Group II	FSUGold, FSUGold4, IU-FSU	0.0021599	-2.02994×10^{-5}	3.76139×10^{-8}	4.64×10^{-12}	-0.99994	3
Group III	Z271s6, Z271s5, Z271s4	0.0063313	-7.69164×10^{-5}	4.53951×10^{-7}	1.41169×10^{-9}	-0.99845	3

TABLE VIII. Characteristics of $(E_{\text{sym},2}^{\text{pot}})^{-2}(n_0)$ vs L_0^{pot} , $(E_{\text{sym},2}^{\text{kin}})^{-2}(n_0)$ vs L_0^{kin} and γ vs $r(n_0)$ regressions for γ_1 . The characteristics of the regressions are the mean square due to regression *MSR*, the mean squared error *MSE*, and the Pearson correlation coefficient $r_{X,Y}$. a , and b are the estimates of the structural parameters of a particular regression model. N_i is the size of the group.

RMF Models		a	b	<i>MSR</i>	<i>MSE</i>	Pearson r_{\cdot}	N_i
$(\hat{E}_{\text{sym},2}^{\text{pot}})^{-2} = a + bL_0^{\text{pot}}$		MeV ⁻²	MeV ⁻³	MeV ⁻⁴	MeV ⁻⁴		
Group Ia	BSR, FSUGZ03, FSUGZ06	0.0060126	-7.57863×10^{-5}	5.75991×10^{-6}	5.05004×10^{-8}	-0.95501	13
Group Ib	BKA, G2*	0.0086623	-0.00016112	1.16554×10^{-6}	1.77416×10^{-7}	-0.87557	4
Group II	FSUGold, FSUGold4, IU-FSU	0.0051507	-6.83135×10^{-5}	7.49779×10^{-7}	1.1468×10^{-8}	-0.99244	3
Group III	Z271s6, Z271s5, Z271s4	0.0038609	-3.65655×10^{-5}	1.02589×10^{-7}	2.60022×10^{-10}	-0.99874	3
$(\hat{E}_{\text{sym},2}^{\text{kin}})^{-2} = a + bL_0^{\text{kin}}$		MeV ⁻²	MeV ⁻³	MeV ⁻⁴	MeV ⁻⁴		
Group Ia	BSR, FSUGZ03, FSUGZ06	0.0043	-1.96191×10^{-5}	1.21959×10^{-8}	3.10725×10^{-10}	-0.88379	13
Group Ib	BKA, G2*	0.0068088	-6.76529×10^{-5}	1.12622×10^{-7}	6.75377×10^{-9}	-0.94494	4
Group II	FSUGold, FSUGold4, IU-FSU	0.0052405	-3.91962×10^{-5}	2.36291×10^{-8}	2.96855×10^{-10}	-0.99378	3
Group III	Z271s6, Z271s5, Z271s4	0.0052381					3
All groups		0.0084653	-0.00010151	9.61737×10^{-6}	1.65674×10^{-8}	-0.98239	23
$\hat{\gamma} = a + br_0$			MeV				
Group Ia	BSR, FSUGZ03, FSUGZ06	2.26262	-2565.16545	0.29432	0.0022886	-0.95979	13
Group Ib	BKA, G2*	0.99671	-595.26274	0.0024162	0.001645	-0.65072	4
Group II	FSUGold, FSUGold4, IU-FSU	1.6318	-1475.4594	0.081895	0.0050426	-0.97057	3
Group III	Z271s6, Z271s5, Z271s4	1.6318	-1475.4594	0.081895	0.0050426	-0.99931	3

the mentioned nonlinear meson interaction terms. The results presented in Fig. 3 reveal an interesting property. The dependencies of $E_{\text{sym},2}(n_b)$ on density, depicted in the left panel in Fig. 3, represent a family of curves similar in shape, with gradually diminishing values for a given density, but this is the $E_{\text{sym},4}(n_b)$ that allows for introducing some systematics in ordering the analyzed models. In the right panel in Fig. 3 the density dependence of $E_{\text{sym},4}(n_b)$ is depicted. The results obtained for the Z272s5 and Z272s6 parametrizations are noteworthy as their $E_{\text{sym},4}(n_b)$ values exceed those obtained for other models. Also, the concavity of the function $E_{\text{sym},4}(n_b)$ for these models is different. The results of further

analysis are represented in a sequence of figures and concern forms of functions $r(n_b)$ and $w(n_b)$. Having obtained the second and fourth-order symmetry-energy functions makes it possible to find a solution to the function $r(n_b)$ determining the specific inaccuracy (Sec. II) of the parabolic approximation. The results are given in the left panel in Fig. 4. This figure shows functions $r(n_b)$ for parametrizations gathered in Table IV. The order in which individual curves appear in Fig. 4 results from the value of the function $r(n_b)$ in n_0 . Details are given in the figure legend. In general, functions $r(n_b)$ are model dependent and do not increase with density. The exception is the group of FSU models, for which some

TABLE IX. Characteristics of $(E_{\text{sym},2}^{\text{pot}})^{-2}(n_0)$ vs L_0^{pot} , $(E_{\text{sym},2}^{\text{kin}})^{-2}(n_0)$ vs L_0^{kin} , and γ vs $r(n_0)$ regressions for γ_2 . The characteristics of the regressions are the mean square due to regression *MSR*, the mean squared error *MSE*, and the Pearson correlation coefficient $r_{X,Y}$. a and b are the estimates of the structural parameters of a particular regression model. N_i is the size of the group.

RMF Models		a	b	<i>MSR</i>	<i>MSE</i>	Pearson r_{\cdot}	N_i
$(\hat{E}_{\text{sym},2}^{\text{pot}})^{-2} = a + bL_0^{\text{pot}}$		MeV ⁻²	MeV ⁻³	MeV ⁻⁴	MeV ⁻⁴		
Group Ia	BSR, FSUGZ03, FSUGZ06	0.0036305	-2.86661×10^{-5}	7.54949×10^{-7}	2.6394×10^{-9}	-0.98131	13
Group Ib	BKA, G2*	0.0054917	-5.84224×10^{-5}	4.3713×10^{-7}	1.58213×10^{-8}	-0.96566	4
Group II	FSUGold, FSUGold4, IU-FSU	0.0032533	-2.7058×10^{-5}	7.17328×10^{-8}	4.28126×10^{-10}	-0.99703	3
Group III	Z271s6, Z271s5, Z271s4	0.0031536	-2.45852×10^{-5}	4.63788×10^{-8}	9.98246×10^{-11}	-0.99893	3
$(\hat{E}_{\text{sym},2}^{\text{kin}})^{-2} = a + bL_0^{\text{kin}}$		MeV ⁻²	MeV ⁻³	MeV ⁻⁴	MeV ⁻⁴		
All groups		0.023890	-0.000736	4.93132×10^{-7}	6.64906×10^{-12}	-0.99986	23
$\hat{\gamma} = a + br_0$			MeV				
Group Ia	BSR, FSUGZ03, FSUGZ06	1.80773	-1460.89946	0.095461	0.00030713	-0.98276	13
Group Ib	BKA, G2*	1.2584	-569.95247	0.0022151	0.00060328	-0.8046	4
Group II	FSUGold, FSUGold4, IU-FSU	1.23879	-676.33617	0.0172085	8.2095×10^{-5}	-0.99762	3
Group III	Z271s6, Z271s5, Z271s4	0.90048	-174.73706	0.013904	2.32044×10^{-5}	-0.99917	3

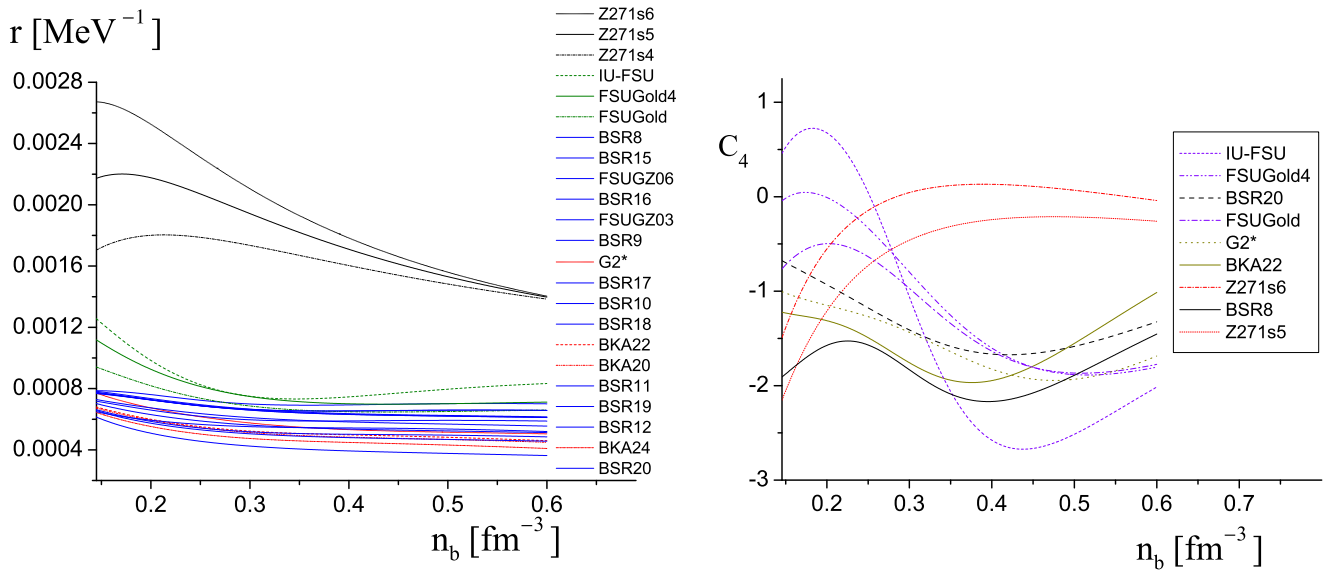


FIG. 4. The left panel presents the parabolic approximation $r(n_b)$ inaccuracy as a function of baryon density n_b calculated for the whole set of parametrizations. The right panel shows the dependence on the density of the correction factors C_4 obtained for the selected parametrizations. The differentiation is evident.

functions $r(n_b)$ have minimum and group of Z272 models for which some functions have maximum. Solving Eq. (18) makes it possible to determine the approximate form of the function $r(n_b)$ denoted in the following by $r^*(n_b)$. This approximate solution is given by Eq. (19). It shows that two factors determine the density dependence of $r^*(n_b)$, the first being the model-specific $L_0/E_{\text{sym},2}(n_0)$ ratio and the second being the correction factor, which reflects the influence of the fourth-order symmetry energy. Calculating the function $r^*(n_b)$ requires determining the value of the C_4 correction factor given by Eq. (20) for the saturation density n_0 . However, the $C_4(n_b)$ dependence is also presented for the results' completeness. The density dependence of $C_4(n_b)$ for the representatives of the distinguished group of models is displayed in the right panel in Fig. 4. The factor that introduces the correction from the fourth-order symmetry energy reveals significantly different density dependencies for parametrizations considered in Fig. 3. The left panel in Fig. 5 shows the approximate solutions to Eq. (19), for all the parametrizations used. The most numerous group are parametrizations for which $r^*(n_b)$ decreases with the density. Three sets of parameters (Group II), for which the dependence on the density is the steepest, deserve mentioning. Although, in this case, the functions $r^*(n_b)$ take large values near the point n_0 , their values decrease quickly with increasing density. Models of Group III show exceptionally high values of $r^*(n_b)$. In the case of the Z271s4 and Z271s5 parametrizations, one observes a further increase with density. An additional advantage of the approximate solution given by Eq. (19) is that the function $r^*(n_b)$ can be determined using the Taylor expansion coefficients of the functions $E_{\text{sym},2}(n_b)$ and $E_{\text{sym},4}(n_b)$ taken at n_0 . The approximate solution given by the exponential function well reproduces the function $r(n_b)$ in a limited density range, close to the saturation value. The left panel in Fig. 5 shows functions $r^*(n_b)$ calculated for the acceptable range of density. In the

case of models belonging to Groups Ia, Ib, and II, the span of this density range is from n_0 to $2n_0$. The comparison of the exact solutions with the approximate one (right panel in Fig. 5) indicates the necessity to truncate the $r^*(n_b)$ solution to a limited range of density. The density range for which the approximate solution is consistent with the exact one is determined by comparing these two functions. The exponential solution is less accurate, especially for densities greater than $2n_0$. The mean approximation error at $n_b = 2n_0$ for the RMF models in the combined Groups Ia, Ib, and II is approximately 10%. The density range encountered in the r^* solution for the Z271s4, Z271s5, and Z271s6 parametrizations is even more narrow due to the approximation error, which in these cases increases significantly with density.

Knowing the function $r(n_b)$ a factor measuring the importance of the $E_{\text{sym},4}(n_b)/E_{\text{sym},2}(n_b)$ the ratio can be determined. It is reasonable to determine the $w(n_b)$ function in the limited density range resulting from the comparison of solutions $r(n_b)$ and $r^*(n_b)$. In that case, $w(n_b)$ can be calculated based on $r^*(n_b)$ function for any density value within this range. The $E_{\text{sym},4}(n_b)/E_{\text{sym},2}(n_b)$ ratio depends decisively on the behavior of the symmetry energy $E_{\text{sym},2}(n_b)$. Within the considered models, the highest values of $w(n_b)$ are for Group III. The specific inaccuracy of the parabolic approximation $r(n_b)$ is closely related to the magnitude of the relative error $w(n_b)$ of this approximation. This can be verified by the relation $r(w)$, which is depicted in the right panel in Fig. 6. For the selected parametrizations in Groups Ia, Ib, and II r decreases with increasing w . The most significant change occurs for densities close to the saturation density. A particular situation arises for the FSUGold4 parametrization for which the steepest change occurs, which can be noticed by comparing the left panel in Fig. 6 and the right panel in Fig. 5 because, in the region where $w(n_b)$ is almost constant, $r(n_b)$ substantially decreases.

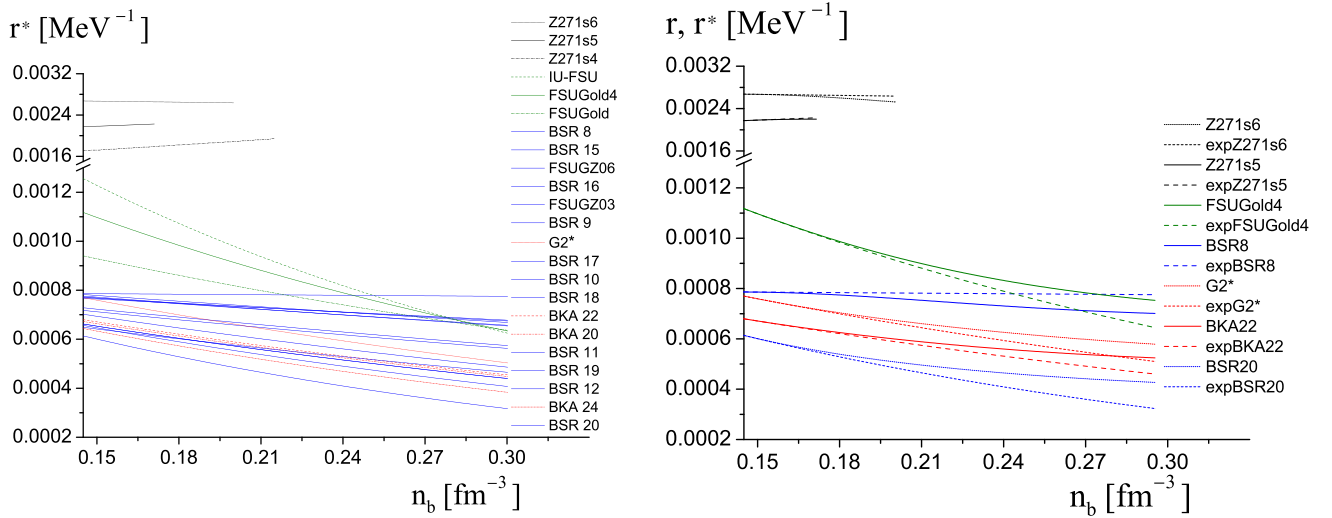


FIG. 5. The left panel shows the approximate solution of Eq. (19), denoted as $r^*(n_b)$, calculated for the entire parametrization set as a function of baryon density n_b . The right panel compares the $r(n_b)$ and $r^*(n_b)$ functions for selected parametrizations. The dashed lines illustrate the obtained exponential solutions $r^*(n_b)$ marked with “exp.”

B. Saturation properties

Analyzing the properties of nuclear matter at the saturation density Table X is of particular importance for confrontation with the existing experimental data. Every adjustment of coupling constants intended to reproduce the coefficients characterizing $E_{\text{sym},2}(n_b)$, in ranges allowed by the experimental limitations, demands the inclusion of a set of constraints. The collection of experimental limitations, presented in the paper of Dutra *et al.* [13,50] and used to specify the appropriate sample of models, is included in Table I. As stated in this table,

the spans of experimental constraints for $E_{\text{sym}}(n_0)$ and L_0 are in the range 25–33 MeV and 25–115 MeV, respectively. Values of $E_{\text{sym},2}(n_0)$ and L_0 obtained for the models considered (parametrizations are given in Table IV) are gathered in the left panels of Figs. 7 and 8. One can see from these figures that the resulting points are scattered in the experimentally allowed areas. The right panel of Fig. 7 shows a specific arrangement of the fourth-order symmetry energy values obtained for the saturation density n_0 . Groups Ia and Ib constitute the most numerous set of models returning relatively similar values of

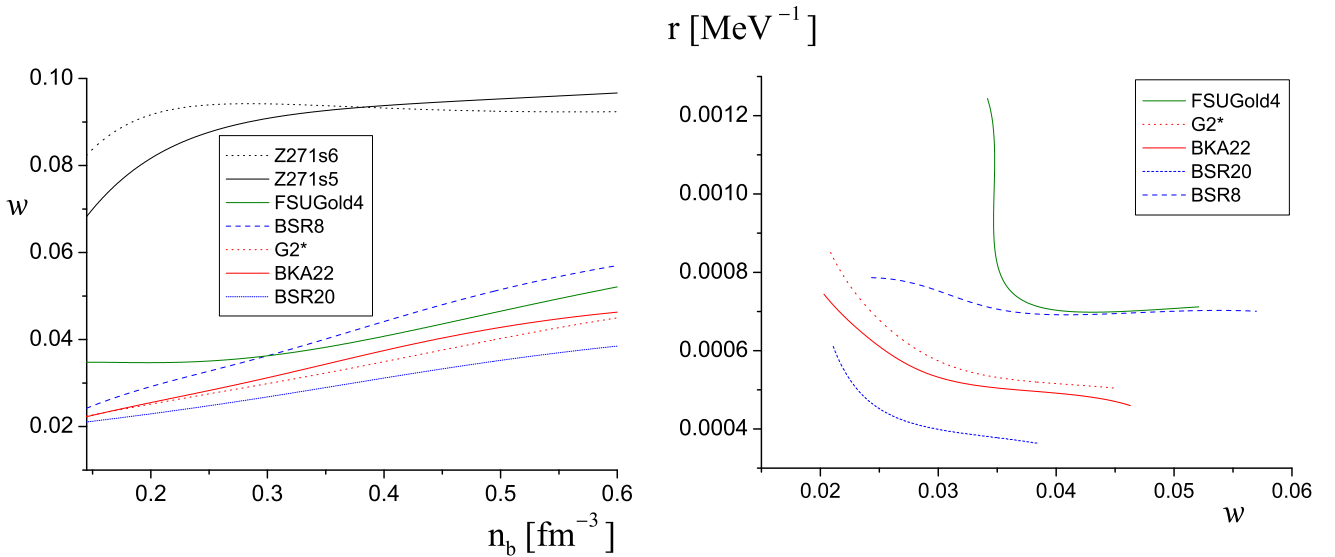


FIG. 6. The left panel shows the density dependence of functions $w(n_b)$, which measures the importance of the fourth-order symmetry energy. The solutions obtained for parametrizations Z271s5 and Z271s6 stand out clearly. $E_{\text{sym},4}(n_b)$ relative to $E_{\text{sym},2}(n_b)$, takes values significantly higher than those obtained for the other models presented in this figure. The distinction is noticeable for the FSUGold4 parametrization because $w(n_b)$ reaches its minimum in the given density range. The right panel shows the relationship between the functions $r(n_b)$ and $w(n_b)$. The specific behavior relates to the FSUGold4 parametrization. In this case, one observes a step change in the value of $r(n_b)$ and its almost constancy afterward.

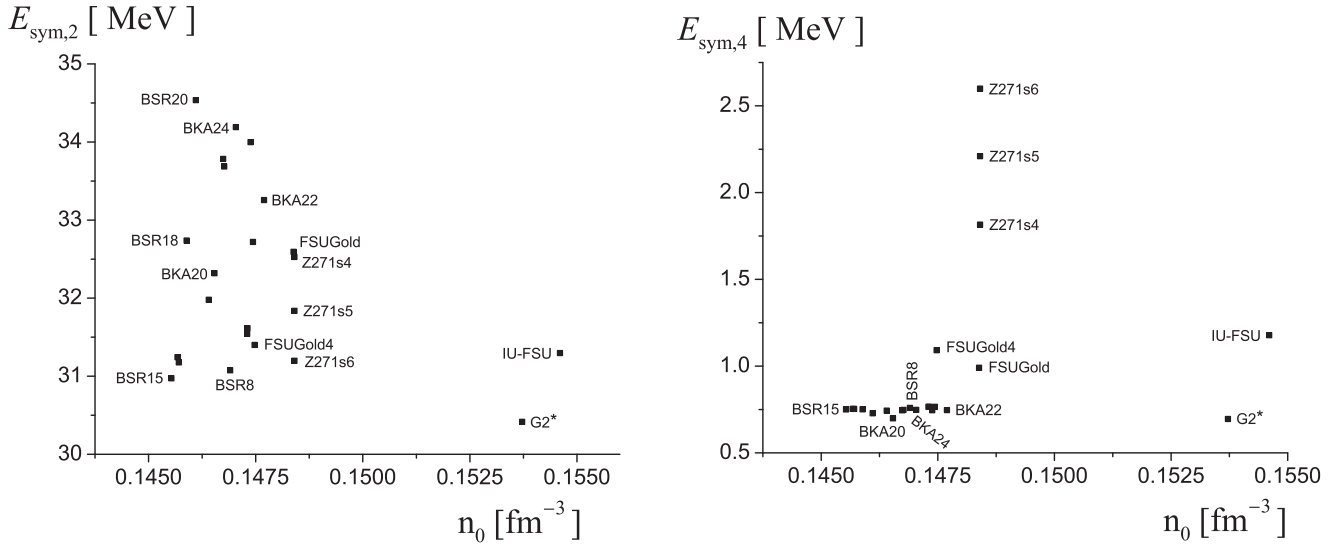


FIG. 7. The symmetry energy $E_{\text{sym},2}(n_0)$ versus saturation density n_0 for selected parametrizations is given in the left panel, whereas the right panel shows the fourth-order symmetry energy $E_{\text{sym},4}(n_0)$ versus n_0 .

$E_{\text{sym},4}(n_0)$. At the same time, significantly different results are obtained for Group II and Group III models. The slope of the fourth-order symmetry energy $L_4 \equiv L_4(n_0)$ (the right panel in Fig. 8) calculated for models belonging to each group shows an arrangement similar to that obtained for $E_{\text{sym},4}(n_0)$ (the right panel in Fig. 7). Figure 9 presents the dependencies of $E_{\text{sym},2}(n_0)$ and $E_{\text{sym},4}(n_0)$ on L_0 . Regression analysis for each group of models separately suggests the possibility of a nonlinear correlation between $E_{\text{sym},2}(n_0)$ and L_0 . This is apparent in the left panel in Fig. 9. The linear regression model for the whole sample produces meaningfully degraded coefficients (see Table V). From the values of the coefficient of determination R^2 given in Table V it can be noticed that the

linear fit for all $N = 23$ RMF models taken together is worse than those obtained within individual groups. It turns out that, for Group Ia, the c coefficient with the L_0^2 factor is statistically significant. However, for the entire sample of $N = 23$ RMF models (Table V), the quadratic term is also statistically significant. Further confirmation that the distinction between groups of models is possible by the analysis of the behavior of the symmetry energy higher-order terms (in this case $E_{\text{sym},4}$) is provided by the right panel in Fig. 9 and by Fig. 10. In the right panel in Fig. 9 the dependence of $E_{\text{sym},4}(n_0)$ on L_0 is presented and Fig. 10, includes the $E_{\text{sym},4}(n_0)$ dependence on $E_{\text{sym},2}(n_0)$. The results of the regression analysis for $E_{\text{sym},4}(n_0)$ vs L_0 and $E_{\text{sym},4}(n_0)$ vs $E_{\text{sym},2}(n_0)$ are summarized in Table VI.

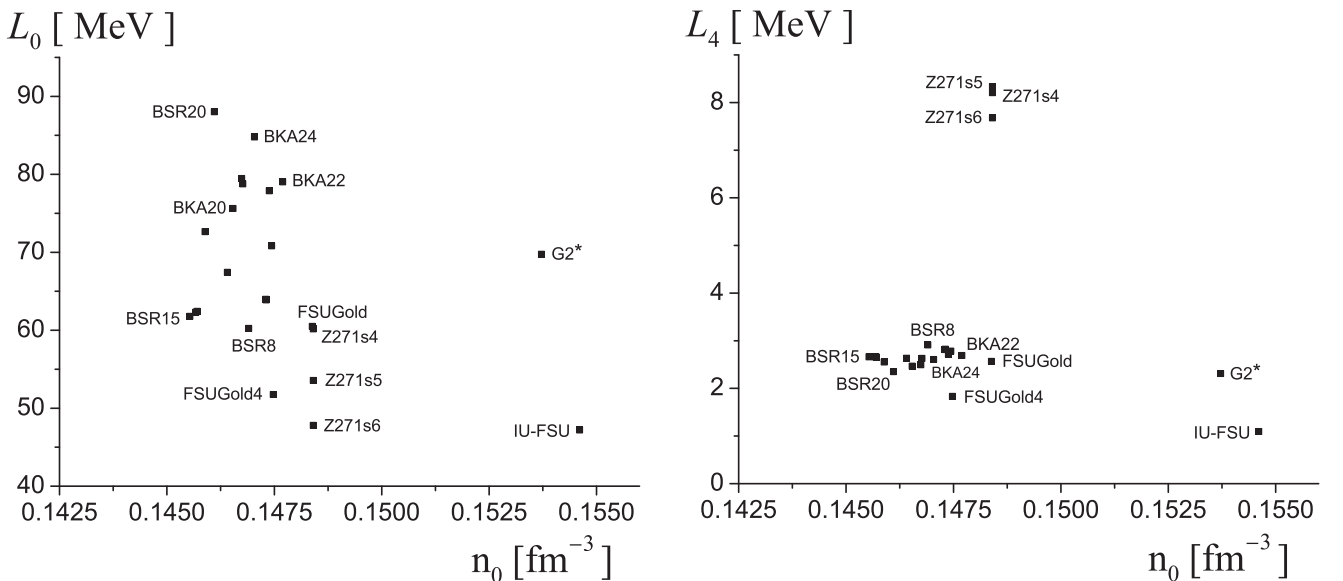


FIG. 8. The same as in Fig. 7 but for the symmetry energy slope L calculated at n_0 [$L(n_0) \equiv L_0$]. The left panel shows the results obtained within the parabolic approximation, and the right depicts the fourth-order symmetry energy slope $L_4(n_0)$ values.

TABLE X. Chosen saturation properties of the asymmetry energy: saturation density n_0 , the second-order $E_{\text{sym},2}(n_0)$ and the fourth-order $E_{\text{sym},4}(n_0)$ symmetry energy coefficients and their slopes L_0 and $L_{0,4}$.

PS	n_0 [fm^{-3}]	$E_{\text{sym},2}(n_0)$ [MeV]	$E_{\text{sym},4}(n_0)$ [MeV]	L_0 [MeV]	$L_{0,4}$ [MeV]
BSR8	0.1469	31.0768	0.7593	60.2507	2.9134
BSR9	0.1473	31.6136	0.7656	63.8931	2.8237
BSR10	0.1474	32.7192	0.7655	70.8318	2.7827
BSR11	0.1468	33.6858	0.7480	78.778	2.6294
BSR12	0.1474	33.9987	0.7460	77.8991	2.7109
BSR15	0.1455	30.9734	0.7504	61.7886	2.6610
BSR16	0.1457	31.2432	0.7536	62.332	2.6629
BSR17	0.1464	31.9794	0.7433	67.4375	2.6338
BSR18	0.1459	32.738	0.7508	72.6483	2.5537
BSR19	0.1467	33.7835	0.7455	79.473	2.4969
BSR20	0.1461	34.5357	0.7284	88.0262	2.3517
FSUGZ03	0.1473	31.5433	0.7654	63.9832	2.8147
FSUGZ06	0.1475	31.1777	0.7538	62.4233	2.6563
BKA20	0.1465	32.3192	0.6994	75.6206	2.4680
BKA22	0.1477	33.2565	0.7466	79.0354	2.6904
BKA24	0.1470	34.1903	0.7477	84.7965	2.6074
G2*	0.1537	30.416	0.6953	69.7508	2.3121
FSUGold	0.1484	32.5931	0.9905	60.498	2.5677
FSUGold4	0.1475	31.401	1.0920	51.7592	1.8335
IU-FSU	0.1546	31.2961	1.1781	47.2041	1.0941
Z272s6	0.1484	31.1982	2.5993	47.8066	7.6791
Z272s5	0.1484	31.8381	2.2101	53.5693	8.3358
Z272s4	0.1484	32.527	1.8159	60.1848	8.2080

Here a comment is in order. The reason for the lower values of the Pearson linear correlation coefficient for Groups Ia and Ib seen in the Table VI is not the badness of the linear fit to the RMF points, but the low sensitivity of the response to the factor change. In other words, the conditional means of $E_{\text{sym},4}(n_0)$ hardly changes with the change of the factor, i.e., either L_0 or $E_{\text{sym},2}(n_0)$. It manifests itself, in particular for

group Ia, by relatively low values of the mean sum of squares due to regression (MSR) and the same order of magnitude of the mean squared error (MSE) when compared with Groups II and III. It can also be noticed (Table VI) that for Group Ib, the sign of the correlations is exceptionally positive.

The specific inaccuracy $r_0 = r(n_b = n_0)$ of the parabolic approximation calculated for saturation densities of individual

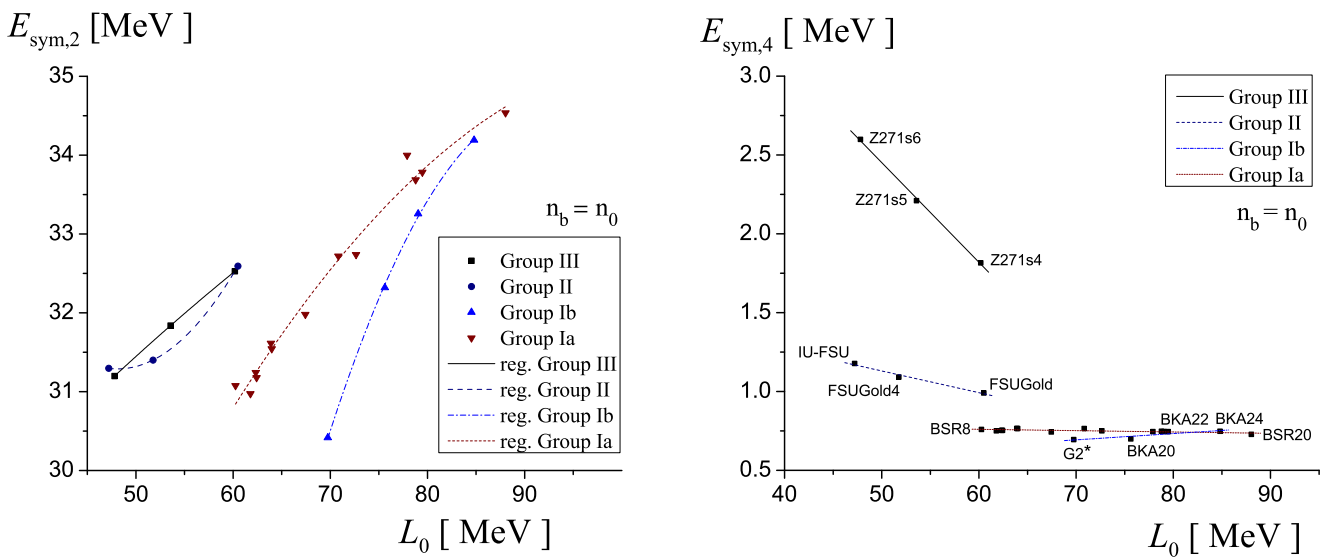


FIG. 9. The left panel shows dependence of $E_{\text{sym},2}(n_0)$ on L_0 . The regression analysis performed for each group of models separately points to the existence of nonlinear correlations between $E_{\text{sym},2}(n_0)$ and L_0 . The right panel depicts the dependence of $E_{\text{sym},4}(n_0)$ on L_0 . The analysis indicates existence of linear correlations between $E_{\text{sym},4}(n_0)$ and L_0 for each group of models.

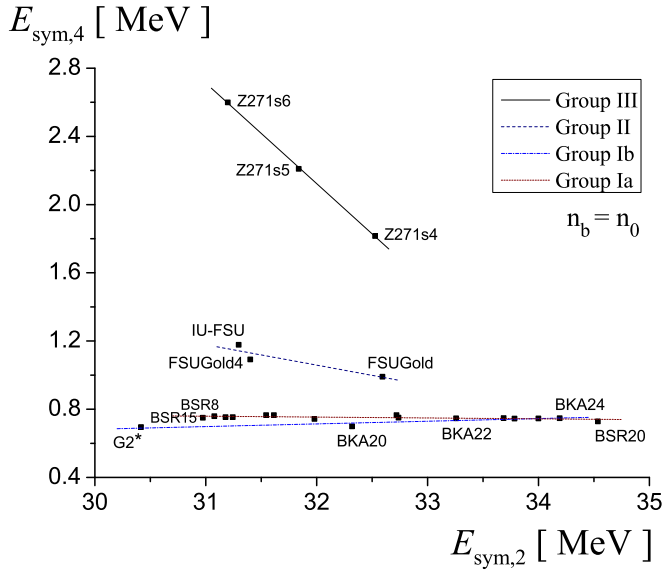


FIG. 10. The dependence of the symmetry energy $E_{\text{sym},4}(n_0)$ on $E_{\text{sym},2}(n_0)$. An ordering of models into separate groups is visible.

models are presented in the left panel in Fig. 11. As in the previous figures, four groups of models can be distinguished. The right panel shows the relationship between the inaccuracy r_0 and the symmetry-energy slope L_0 . The regression of r_0 vs L_0 , in the four groups of RMF models separately, shows that within a given group the models lie very close to the straight regression line (see Table VII). The dependence of the symmetry energy on density significantly influences the function $r(n_b)$, which is reflected in the reliance of conditional means \hat{r}_0 on L_0 . The values of the Pearson correlation coefficient $r_{r_0 L_0}$, shown in Table VII, signifies that the linear correlation between these variables is negative and very strong. The right panel in Fig. 11 shows the effect of the slope of symmetry

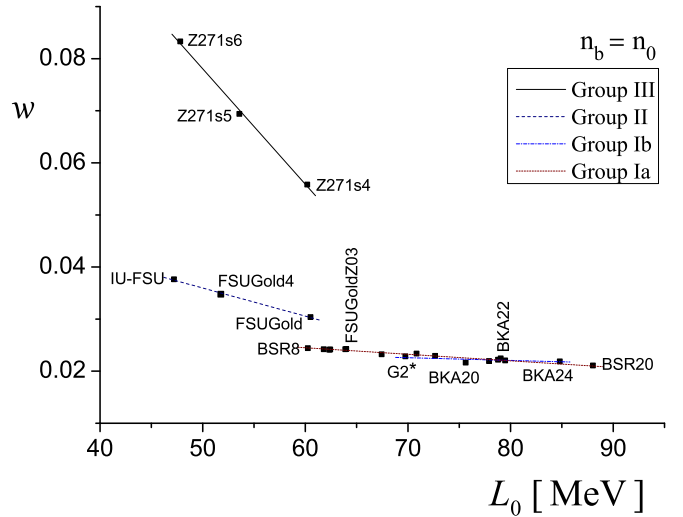
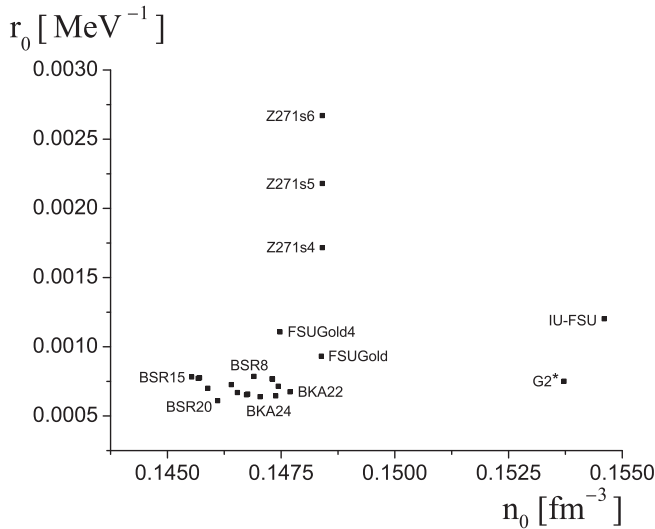


FIG. 12. The factor $w \equiv w(n_0)$ determining the $E_{\text{sym},4}$ relative to $E_{\text{sym},2}$ versus L_0 . For each group, the highest value of w is achieved for the lowest value of L_0 .

energy on the r_0 values. For each group of models, the highest value of r_0 is obtained for the smallest value of L_0 . A similar conclusion can be drawn when analyzing the dependence of the $w(n_0)$ coefficient on L_0 within each group (Table VII, Fig. 12), one can notice the characteristic behavior of the w factor, which has the highest value for the models with the lowest L_0 value. The function $r(n_b)$ can be treated as a physical quantity that has been derived under the assumption that the symmetry energy is well approximated by the Padé approximant method. Then recalling the strong linear correlation between r_0 and L_0 and using the regression function $\hat{r}_0 = a + bL_0$, one can suggest the condition that in accord with Eq. (12) must be imposed on the function that describes the energy of the

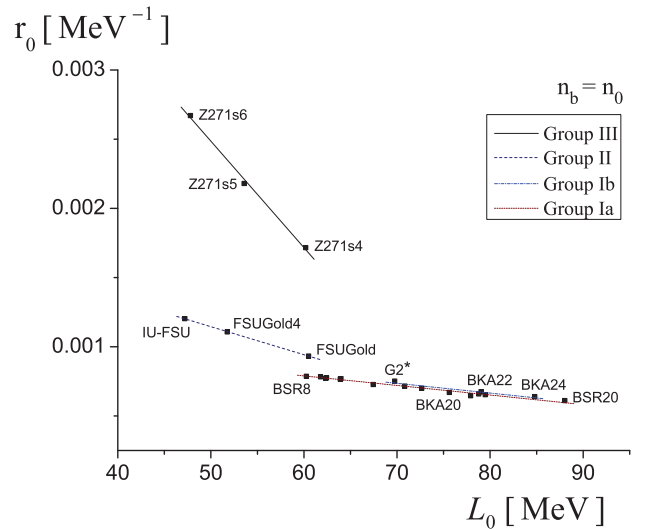


FIG. 11. The left panel gives the values of the parabolic approximation $r(n_0) \equiv r_0$ incorrectness calculated at the saturation densities n_0 . The right panel depicts the parabolic approximation r_0 incorrectness versus the symmetry energy slope L_0 . In this case, the individual mode represented by points concentrated along straight lines confirms the existence of the selected groups.

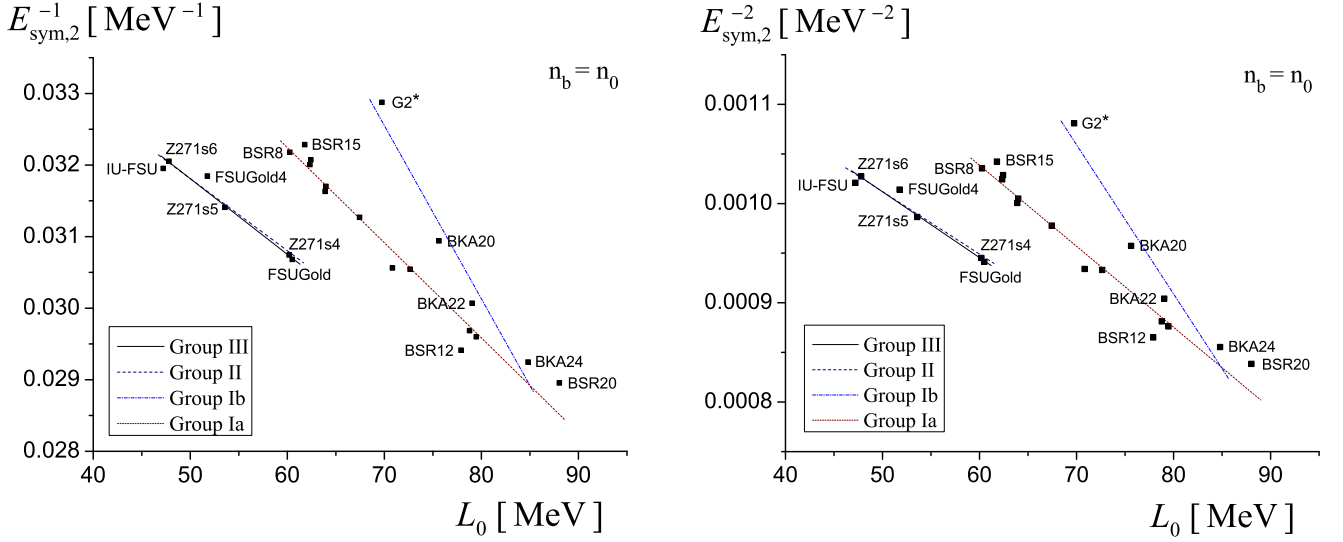


FIG. 13. Dependence of $E_{\text{sym},2}^{-2}$ on the symmetry energy slope L_0 . Linear regression analysis shows a relationship between $E_{\text{sym},2}^{-2}$ and L_0 for models belonging to each group.

system

$$\begin{aligned} & \frac{\partial^4 E(n_0, \delta)}{\partial \delta^4} \Big|_{\delta=0} \left(\frac{\partial^2 E(n_0, \delta)}{\partial \delta^2} \Big|_{\delta=0} \right)^{-2} \\ & = a + 3n_0 b \frac{\partial}{\partial n_b} \left(\frac{\partial^2 E(n_b, \delta)}{\partial \delta^2} \Big|_{\delta=0} \right) \Big|_{n_b=n_0}. \end{aligned} \quad (49)$$

As discussed previously, the conditional mean of $E_{\text{sym},4}$ changes linearly with L_0 , and $E_{\text{sym},4}$ is in the nominator on the LHS of Eq. (49). The factor $E_{\text{sym},2}^{-2}$ besides $E_{\text{sym},4}$ on the LHS of Eq. (49) is dominant in determining the parabolic approx-

imation specific inaccuracy r . Thus, it is also interesting to investigate its dependence on L_0 . In accord with the values in Table VI, the results shown in Fig. 13 point again to the very good linear correlation between the quantities $E_{\text{sym},2}^{-2}$ and L_0 for each group of models. The correlation between r_0 and L_0 is very good (see Table VII). This, together with the premises of Padé analysis mentioned just above, gives additional support for proposing Eq. (49) as the physical bound on the energy density in the modeling the generalized, future RMF models. Nevertheless, one can consider in Eq. (49) the extension of the regression analysis by inclusion higher-order terms of L_0 in

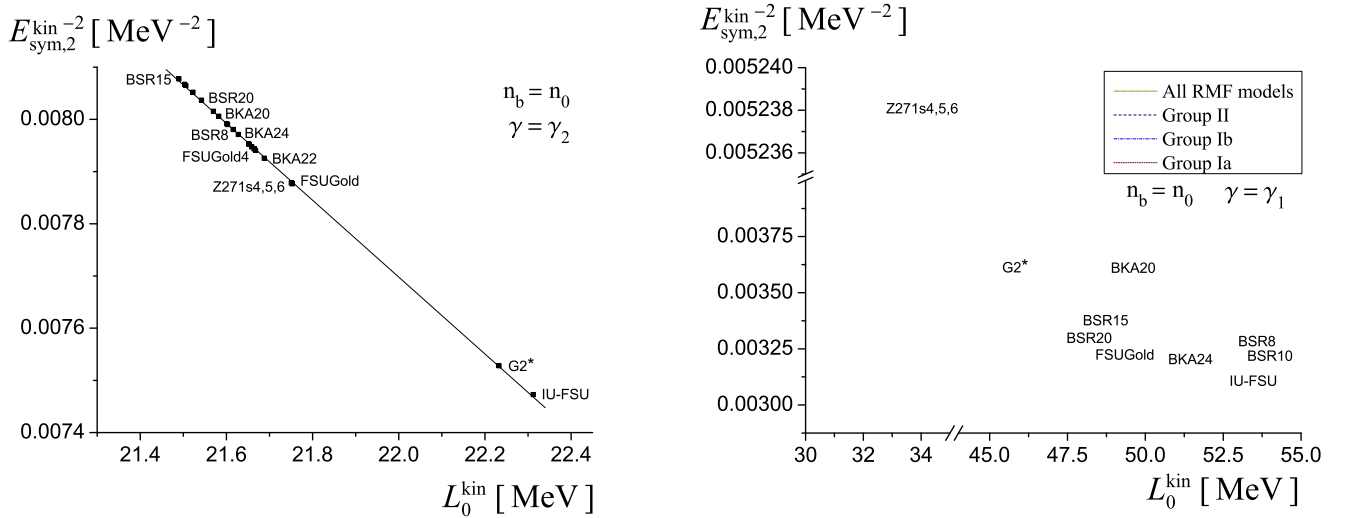


FIG. 14. The left panel reveals the exact linear correlation between the kinetic components $E_{\text{sym},2}^{\text{kin}-2}(n_0)$ and L_0^{kin} for the case where the kinetic part of the symmetry energy does not involve interaction with the scalar meson σ ; thus, without medium modified nucleon mass. When the power-law parametrizes the dependence of the symmetry energy on density, the case under consideration corresponds to the γ_2 coefficient. The right panel shows the results of the same analysis performed for the γ_1 case. The linear correlations between $E_{\text{sym},2}^{\text{kin}-2}(n_0)$ and L_0^{kin} were obtained separately for each group.

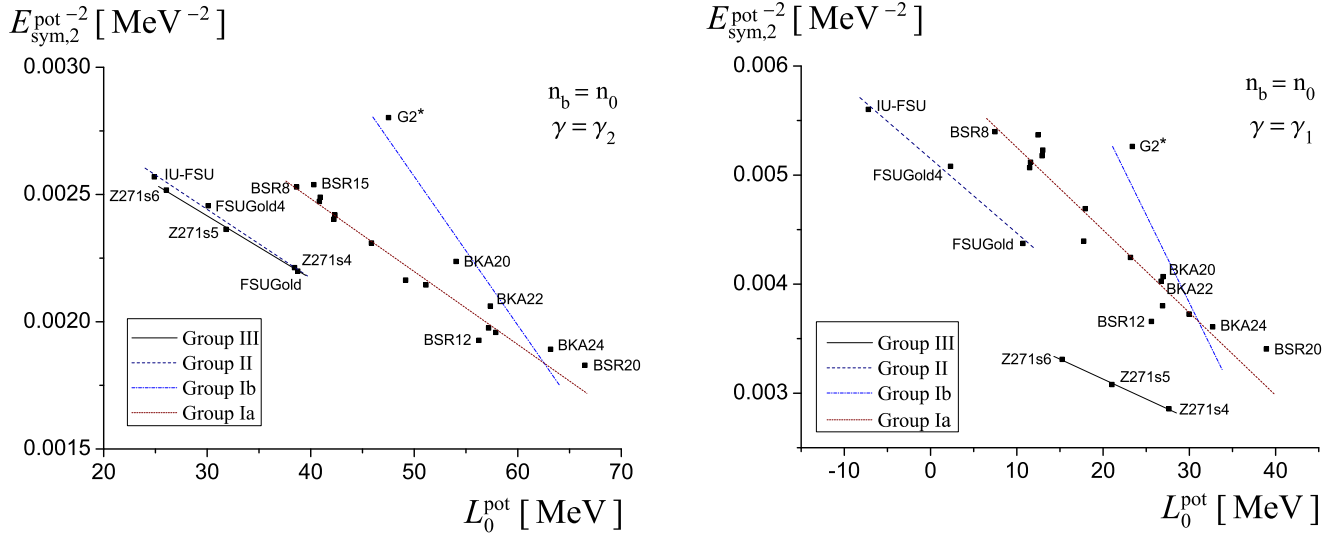


FIG. 15. The linear regression analysis performed for the potential part of the symmetry energy. The left panel shows results obtained for the γ_2 case and the right panel for the γ_1 . In both cases, linear correlations were obtained separately among each group of models.

the regression functions of r_0 , $E_{\text{sym},4}$ and $E_{\text{sym},2}^{-2}$. Additionally, the utility of $E_{\text{sym},2}^{-2}$ in the analysis of the RMF models is due to the very good fit of the linear regression $E_{\text{sym},2}^{-2}$ vs L_0 in each group of models (see Table VI). The same is true for the linear regression $E_{\text{sym},2}^{-1}$ vs L_0 (see Table VI) and the squared of $E_{\text{sym},2}^{-1}$ can be used instead of $E_{\text{sym},2}^{-2}$ as a multiplier of $E_{\text{sym},4}$ in Eq. (49). An analysis of the kinetic $E_{\text{sym},2}^{\text{kin}-2}$ and potential $E_{\text{sym},2}^{\text{pot}-2}$ terms for the energy symmetry can also be performed (Tables XI–XIII). The results of the corresponding regression analyses are collected in Tables VIII and IX. When the kinetic

part is given by Eq. (33), then there is a functional relationship between $E_{\text{sym},2}^{\text{kin}-2}$ and L_0 . In this case, the regression analysis results in the straight line shown in the left panel in Fig. 14. With the assumption that the kinetic-energy contribution to the symmetry energy includes the effective nucleon mass, the obtained regression lines can be fit separately for each group of models, which is shown in the right panel in Fig. 14. The determined linear correlation coefficients are given in Table VIII. Results of the linear regression analysis performed for the dependence of the potential symmetry energy $E_{\text{sym},2}^{\text{pot}-2}$ on L_0 is presented in Fig. 15. When the potential energy of the

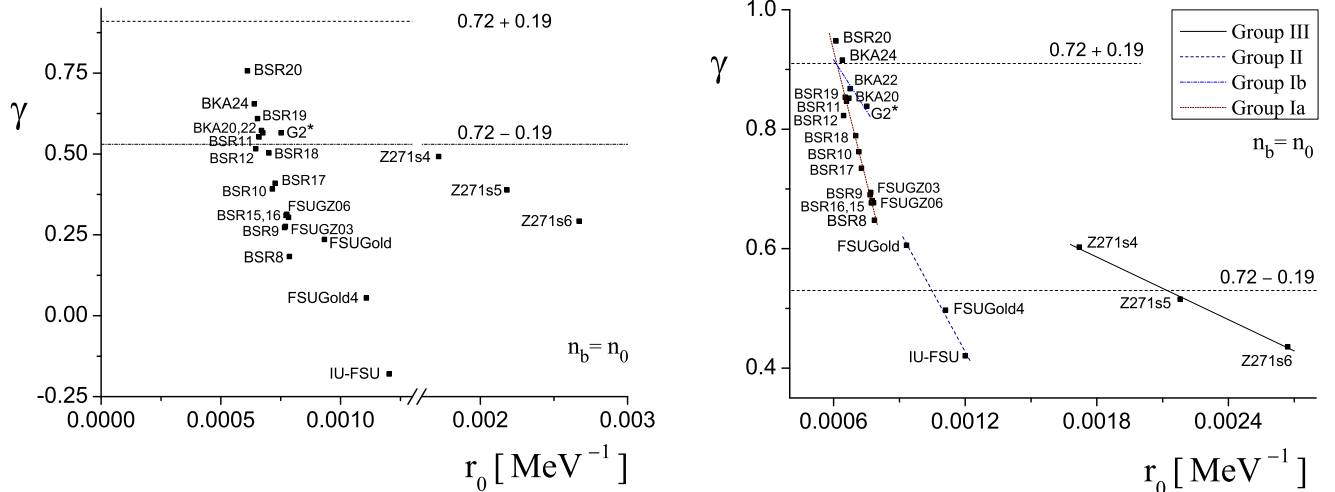


FIG. 16. This figure presents the dependence of γ parameter determining the power-law parametrization of the symmetry energy on the incorrectness factor $r(n_b)$. The analysis was carried out for selected density values being multiples of n_0 . A detailed analysis of the diagram is given in the text. The left panel contains the results for γ_1 and the right panel for γ_2 . Horizontal solid lines limit the experimentally accessible range of γ .

TABLE XI. Decomposition of the symmetry energy and its slope into the kinetic and potential parts. Values of particular coefficients are taken at saturation density n_0 . The kinetic part includes the effective nucleon mass $M_{\text{eff}} = M - g_\sigma s$.

PS	$E_{\text{sym},2}^{\text{kin}}(n_0)$ [MeV]	$E_{\text{sym},2}^{\text{pot}}(n_0)$ [MeV]	L_0^{kin} [MeV]	L_0^{pot} [MeV]	γ_1
BSR8	17.4661	13.6107	52.7778	7.47294	0.18
BSR9	17.5668	14.0468	52.4064	11.4867	0.27
BSR10	17.6339	15.0853	53.0864	17.7454	0.39
BSR11	17.4679	16.218	51.891	26.887	0.55
BSR12	17.4655	16.5332	52.3014	25.5977	0.52
BSR15	17.3255	13.6479	49.3392	12.4494	0.30
BSR16	17.3453	13.8979	49.4071	12.9249	0.31
BSR17	17.3803	14.5991	49.503	17.9345	0.41
BSR18	17.3896	15.3483	49.4802	23.1681	0.50
BSR19	17.4007	16.3828	49.5144	29.9586	0.61
BSR20	17.3999	17.1358	49.0976	38.9287	0.76
FSUGZ03	17.5657	13.9776	52.4026	11.5806	0.28
FSUGZ06	17.3491	13.8287	49.419	13.0043	0.31
BKA20	16.6426	15.6766	48.6818	26.9389	0.57
BKA22	17.4975	15.7591	52.313	26.7224	0.57
BKA24	17.5426	16.6477	52.0947	32.7019	0.65
G2*	16.6317	13.7843	46.366	23.3847	0.57
FSUGold	17.471	15.1221	49.7934	10.7046	0.24
FSUGold4	17.3707	14.0303	49.4458	2.31333	0.05
IU-FSU	17.9358	13.3604	54.4133	-7.20916	-0.18
Z272s6	13.817	17.3811	32.5519	15.2547	0.29
Z272s5	13.817	18.021	32.5519	21.0174	0.39
Z272s4	13.817	18.71	32.552	27.6327	

TABLE XII. Decomposition of the symmetry energy and its slope into the kinetic and potential parts. Values of particular coefficients are taken at the saturation density n_0 . The kinetic part does not include the medium modification of the nucleon mass.

PS	$E_{\text{sym},2}^{\text{kin}}(n_0)$ [MeV]	$E_{\text{sym},2}^{\text{pot}}(n_0)$ [MeV]	L_0^{kin} [MeV]	L_0^{pot} [MeV]	γ_2
BSR8	11.1939	19.8828	21.6154	38.6353	0.65
BSR9	11.2139	20.3998	21.6525	42.2406	0.69
BSR10	11.2201	21.499	21.6642	49.1676	0.76
BSR11	11.1872	22.4986	21.6028	57.1752	0.85
BSR12	11.2174	22.7813	21.659	56.2401	0.82
BSR15	11.1266	19.8468	21.4898	40.2989	0.62
BSR16	11.1336	20.1096	21.5029	40.8291	0.68
BSR17	11.1695	20.8099	21.5698	45.8677	0.73
BSR18	11.1441	21.5939	21.5224	51.126	0.79
BSR19	11.1859	22.5975	21.6004	57.8726	0.85
BSR20	11.1547	23.381	21.5422	66.4841	0.95
FSUGZ03	11.2134	20.3298	21.6516	42.3315	0.69
FSUGZ06	11.1352	20.0426	21.5058	40.9175	0.68
BKA20	11.1761	21.1431	21.5821	54.0385	0.85
BKA22	11.2327	22.0238	21.6877	57.3477	0.87
BKA24	11.2005	22.9899	21.6275	63.169	0.92
G2*	11.5254	18.8906	22.2326	47.5182	0.84
FSUGold	11.2664	21.3267	21.7504	38.7476	
FSUGold4	11.222	20.179	21.6676	30.0916	0.50
IU-FSU	11.568	19.7282	22.3119	24.8922	
Z272s6	11.2675	19.9307	21.7524	26.0542	0.44
Z272s5	11.2675	20.5706	21.7524	31.8169	0.52
Z272s4	11.2657	21.2596	21.7524	38.4324	0.60

symmetry energy is expressed by Eq. (34) (the left panel in Fig. 15) as well as when it is given by Eq. (31) (the right panel in Fig. 15) four groups of models can be distinguished. Linear regression analysis was performed for each of these groups.

C. Power-law parametrization of the symmetry energy

An alternative method of symmetry energy parametrization using the power law to its description allows referring to the obtained experimental constraints. Results reported by Russotto [71] led to an estimate of the γ exponent, which after including all corrections, 1σ statistical uncertainty and systematic uncertainties take the value at 0.72 ± 0.19 . This corresponds to the value of the slope parameter $L_0 = 72 \pm 13$ MeV. Figure 16 shows the γ parameter's dependence on the $r_0 = r(n_0)$ coefficient, characterizing the parabolic approximation's inaccuracy. The obtained distribution of points determined for all parametrizations leads to a noticeably different behavior for the distinguished groups of models. Models of Groups Ia and Ib are characterized by a higher value of γ , which is consonant with a higher value of L_0 . The horizontal lines correspond to experimentally acceptable values of γ . The right panel shows the dependence of γ_2 on r_0 . It is easy to notice that the distribution of points for individual models is analogous to that obtained for γ_1 —but the values of γ_2 are greater than γ_1 . This change is due to the different forms of the kinetic and the potential parts of the symmetry energy. The effect of γ redefinition increases the number of models yielding results within experimentally acceptable values. From Tables VIII and IX it can be noticed that the linear regression fit of γ vs r_0 for γ_2 is better than γ_1 except for Group III (where there is a very small difference). The case of γ_2 also gives the smallest value of the Akaike information criterion obtained in Sec. IV B 2, Table II. These facts suggest that the splitting of L_0 followed by Eq. (36), and therefore the one that is consistent with the method used in the case of γ_2 better suits the actual situation.

VI. CONCLUSIONS

The EoS of nuclear matter encodes information about the symmetry energy, which is assigned a vital role in the structure of both neutron-rich nuclei and neutron stars. The parabolic approximation is a commonly used method to describe the symmetry energy. This paper presents an approach that estimates the significance of the symmetry energy quartic term. It was found that the measure of the importance of the $w(n_b) = E_{\text{sym},4}(n_b)/E_{\text{sym},2}(n_b)$ ratio and the related function called specific inaccuracy of the parabolic approximation $r(n_b)$ depend on the density. Their values also depend decisively on the form of the symmetry energy and can be estimated for any density value within the admissible range, which for most models is $(n_0, 2n_0)$. An important fact is that in this density range, the value of $E_{\text{sym},4}(n_b)/E_{\text{sym},2}(n_b)$ ratio can be determined based only on the coefficients characterizing the form of the symmetry energy at saturation density n_0 . The analysis of the function determining the specific inaccuracy of the parabolic approximation made it possible to notice a kind of ordering in the whole class of the considered models. All models, carefully selected according to the experimental constraints used for the analysis, representing different experimental situations. The two-dimensional regression analysis of model selection based on the Akaike information criterion is presented. The results of this analysis indicates that all the considered models are consistent with Eq. (30), which results from adopting the power-law parametrization of the symmetry energy. It turns out that the Akaike information criterion is sensitive to how the symmetry energy of the model is decomposed into kinetic and potential parts. On the other hand, after conducting a series of one-dimensional regression analyzes, it turned out that the RMF models do not form a chaotic set in the input parameters space ($E_{\text{sym},2}$, L_0 , $E_{\text{sym},4}$, L_4 , n_b , etc.), but four groups of models. In each of these groups, the RMF models are represented by regression functions for these input parameters with characteristics suggesting linear relationship in the class of RMF models.

-
- [1] J. M. Lattimer and M. Prakash, *Science* **304**, 536 (2004).
 [2] P. Danielewicz, R. Lacey, and W. G. Lynch, *Science* **298**, 1592 (2002).
 [3] A. W. Steiner, M. Prakash, J. M. Lattimer, and P. J. Ellis, *Phys. Rep.* **411**, 325 (2005).
 [4] C. J. Horowitz, E. F. Brown, Y. Kim, W. G. Lynch, R. Michaels, A. Ono, J. Piekarewicz, M. B. Tsang, and H. H. H. Wolter, *J. Phys. G* **41**, 093001 (2014).
 [5] Y. Zhang, P. Danielewicz, M. Famiano, Z. Li, W. G. Lynch, and M. B. Tsang, *Phys. Lett. B* **664**, 145 (2008).
 [6] M. Zielinska-Pfabe, *Acta Phys. Pol. B Proc. Suppl.* **10**, 153 (2017).
 [7] M. Oertel, M. Hempel, T. Klöhn, and S. Typel, *Rev. Mod. Phys.* **89**, 015007 (2017).
 [8] B.-A. Li, P. G. Krastev, D.-H. Wen, and N.-B. Zhang, *Eur. Phys. J. A* **55**, 117 (2019).
 [9] K. Sumiyoshi, K. Nakazato, H. Suzuki, J. Hu, and H. Shen, *Astrophys. J. Lett.* **887**, 110 (2019).
 [10] B. D. Serot and J. D. Walecka, The relativistic nuclear anybody problem, in *Advances in Nuclear Physics*, edited by J. W. Negele and E. Vogt (Plenum, New York, 1986), Vol. 16.
 [11] B. D. Serot and J. D. Walecka, *Int. J. Mod. Phys. E* **06**, 515 (1997).
 [12] J. Boguta and A. R. Bodmer, *Nucl. Phys. A* **292**, 413 (1977).
 [13] M. Dutra, O. Lourenço, S. S. Avancini, B. V. Carlson, A. Delfino, D. P. Menezes, C. Providência, S. Typel, and J. R. Stone, *Phys. Rev. C* **90**, 055203 (2014).
 [14] I. Bednarek, R. Manka, and M. Pienkos, *PLoS ONE* **9**, e106368 (2014).
 [15] V. Baran, M. Colonna, V. Greco, and M. Di Toro, *Phys. Rep.* **410**, 335 (2005).
 [16] L. W. Chen, C. M. Ko, B.-A. Li, and G. C. Yong, *Front. Phys. Chin.* **2**, 327 (2007).
 [17] J. W. Holt and Y. Lim, *Phys. Lett. B* **784**, 77 (2018).
 [18] J. M. Pearson, N. Chamel, A. F. Fantina, and S. Goriely, *Eur. Phys. J. A* **50**, 43 (2014).

- [19] L.-W. Chen, Ch. M. Ko, and B.-A. Li, *Phys. Rev. C* **72**, 064309 (2005).
- [20] M. B. Tsang, T. X. Liu, L. Shi, P. Danielewicz, C. K. Gelbke, X. D. Liu, W. G. Lynch, W. P. Tan, G. Verde, A. Wagner, H. S. Xu, W. A. Friedman, L. Beaulieu, B. Davin, R. T. de Souza, Y. Larochelle, T. Lefort, R. Yanez, V. E. Viola Jr., R. J. Charity, and L. G. Sobotka, *Phys. Rev. Lett.* **92**, 062701 (2004).
- [21] P. Danielewicz and J. Lee, *Nucl. Phys. A* **922**, 1 (2014).
- [22] Z. Chen, S. Kowalski, M. Huang, R. Wada, T. Keutgen *et al.*, *Phys. Rev. C* **81**, 064613 (2010).
- [23] Z. Z. Li, Y. F. Niu, and W. H. Long, *Phys. Rev. C* **103**, 064301 (2021).
- [24] J. Piekarewicz, *Eur. Phys. J. A* **50**, 25 (2014).
- [25] X.-H. Li, B.-J. Cai, L.-W. Chen, R. Chen, B.-A. Li, and Ch. Xu, *Phys. Lett. B* **721**, 101 (2013).
- [26] B.-A. Li, *Nucl. Phys. News* **27**, 7 (2017).
- [27] T.-G. Yue, L.-W. Chen, Z. Zhang, and Y. Zhou, *Phys. Rev. Res.* **4**, L022054 (2022).
- [28] D. Adhikari *et al.* (PREX Collaboration), *Phys. Rev. Lett.* **126**, 172502 (2021).
- [29] S. Abrahamyan *et al.* (PREX Collaboration), *Phys. Rev. Lett.* **108**, 112502 (2012).
- [30] Z. Zhang and L. W. Chen, *Phys. Lett. B* **726**, 234 (2013).
- [31] B. G. Todd-Rutel and J. Piekarewicz, *Phys. Rev. Lett.* **95**, 122501 (2005).
- [32] F. J. Fattoyev, J. Piekarewicz, and C. J. Horowitz, *Phys. Rev. Lett.* **120**, 172702 (2018).
- [33] Y. Zhou, L. W. Chen, and Z. Zhang, *Phys. Rev. D* **99**, 121301(R) (2019).
- [34] Y. Zhou and L. W. Chen, *Astrophys. J. Lett.* **886**, 52 (2019).
- [35] M. B. Tsang, Y. Zhang, P. Danielewicz, M. Famiano, Z. Li, W. G. Lynch, and A. W. Steiner, *Phys. Rev. Lett.* **102**, 122701 (2009).
- [36] A. W. Steiner, J. M. Lattimer, and E. F. Brown, *Astrophys. J.* **722**, 33 (2010).
- [37] B.-A. Li and X. Han, *Phys. Lett. B* **727**, 276 (2013).
- [38] B. A. Li, L. W. Chen, and C. M. Ko, *Phys. Rep.* **464**, 113 (2008).
- [39] B. J. Cai, F. J. Fattoyev, B. A. Li, and W. G. Newton, *Phys. Rev. C* **92**, 015802 (2015).
- [40] G. A. Baker Jr. and P. R. Graves-Morris, *Padé Approximants*, 2nd ed. (Cambridge University Press, Cambridge, 1996).
- [41] H. Akaike, *IEEE Trans. Autom. Control*, **19**, 716 (1974).
- [42] J. Xu, L.-W. Chen, B.-A. Li, and H.-R. Ma, *Astrophys. J.* **697**, 1549 (2009).
- [43] O. Lourenço, M. Dutra, and D. P. Menezes, *Phys. Rev. C* **95**, 065212 (2017).
- [44] B. J. Cai and L. W. Chen, *Phys. Rev. C* **85**, 024302 (2012).
- [45] O. L. Ibryaeva and V. M. Adukov, *J. Comp. App. Math.* **237**, 529 (2013).
- [46] I. Bednarek, J. Śladkowski, and J. Syska, *J. Phys. Soc. Jpn.* **88**, 124201 (2019).
- [47] I. Bednarek, J. Śladkowski, and J. Syska, *Symmetry* **12**, 898 (2020).
- [48] H. Müller and B. D. Serot, *Nucl. Phys. A* **606**, 508 (1996).
- [49] C. J. Horowitz and J. Piekarewicz, *Phys. Rev. Lett.* **86**, 5647 (2001).
- [50] M. Dutra, O. Lourenço, O. Hen, E. Piaseckzy, and D. P. Menezes, *Chin. Phys. C* **42**, 064105 (2018).
- [51] J. R. Stone, N. J. Stone, and S. A. Moszkowski, *Phys. Rev. C* **89**, 044316 (2014).
- [52] E. Khan, J. Margueron, and I. Vidana, *Phys. Rev. Lett.* **109**, 092501 (2012).
- [53] E. Khan and J. Margueron, *Phys. Rev. C* **88**, 034319 (2013).
- [54] M. Farine, J. M. Pearson, and F. Tondeur, *Nucl. Phys. A* **615**, 135 (1997).
- [55] W. G. Lynch, M. B. Tsang, Y. Zhang, P. Danielewicz, M. Famiano, Z. Li, and A. W. Steiner, *Prog. Part. Nucl. Phys.* **62**, 427 (2009).
- [56] J. R. Stone and P. G. Reinhard, *Prog. Part. Nucl. Phys.* **58**, 587 (2007).
- [57] M. B. Tsang, J. R. Stone, F. Camera, P. Danielewicz, S. Gandolfi, K. Hebeler, C. J. Horowitz, J. Lee, W. G. Lynch, Z. Kohley, R. Lemmon, P. Moller, T. Murakami, S. Riordan, X. Roca-Maza, F. Sammarruca, A. W. Steiner, I. Vidaña, and S. J. Yennello, *Phys. Rev. C* **86**, 015803 (2012).
- [58] B.-A. Li *et al.*, *J. Phys.: Conf. Ser.* **312**, 042006 (2011).
- [59] M. Centelles, X. Roca-Maza, X. Viñas, and M. Warda, *Phys. Rev. Lett.* **102**, 122502 (2009).
- [60] T. Li, U. Gang, Y. Liu, R. Marks, B. Nayak, B. K. Madhusudhana *et al.*, *Phys. Rev. Lett.* **99**, 162503 (2007).
- [61] P. Danielewicz, *Nucl. Phys. A* **727**, 233 (2003).
- [62] S. K. Dhiman, R. Kumar, and B. K. Agrawal, *Phys. Rev. C* **76**, 045801 (2007).
- [63] R. Kumar, B. K. Agrawal, and S. K. Dhiman, *Phys. Rev. C* **74**, 034323 (2006).
- [64] B. K. Agrawal, *Phys. Rev. C* **81**, 034323 (2010).
- [65] A. Sulaksono and T. Mart, *Phys. Rev. C* **74**, 045806 (2006).
- [66] J. Piekarewicz and S. P. Weppner, *Nucl. Phys. A* **778**, 10 (2006).
- [67] F. J. Fattoyev, C. J. Horowitz, J. Piekarewicz, and G. Shen, *Phys. Rev. C* **82**, 055803 (2010).
- [68] C. J. Horowitz and J. Piekarewicz, *Phys. Rev. C* **66**, 055803 (2002).
- [69] Y. Pawitan, *In all Likelihood: Statistical Modelling and Inference using Likelihood* (Oxford University Press, New York, 2001).
- [70] D. G. Kleinbaum, L. L. Kupper, K. E. Muller, and A. Nizam, *Applied Regression Analysis and Other Multivariable Method* (Duxbury Press, Pacific Grove, 1998).
- [71] P. Russotto *et al.*, *Phys. Rev. C* **94**, 034608 (2016).